

AD-A059 812

ARIZONA UNIV TUCSON

EXCITATION OF A WIRE IN A RECTANGULAR CAVITY. VOLUME I. THEORY. (U)

F/G 20/14

MAY 78 D B SEIDEL

AFOSR-76-3009

UNCLASSIFIED

AFWL-TR-77-221-VOL-1

NL

2
OF
AD
A069812



28 2.5
12 2.2
6 2.0
2 1.8
1.6

812

F



DDC FILE COPY AD A059812



A

AFWL-TR-77-221

DDC

AFWL-TR
77-221

ADE300164

② **LEVEL** III

A050073

AD A059812

DDC FILE COPY



EXCITATION OF A WIRE IN A RECTANGULAR CAVITY

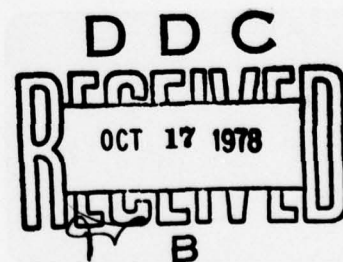
Volume I: THEORY

University of Arizona
Tucson, AZ 85724

May 1978

Final Report

Approved for public release; distribution unlimited.



AIR FORCE WEAPONS LABORATORY
Air Force Systems Command
Kirtland Air Force Base, NM 87117

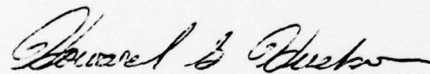
78 09 05 127

This final report was prepared by the University of Arizona, Tucson, Arizona, through AFOSR Grant 76-3009, Job Order 12090525 with the Air Force Weapons Laboratory, Kirtland Air Force Base, New Mexico. Capt Howard G. Hudson (ELT) was the Laboratory Project Officer-in-Charge.

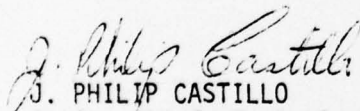
When US Government drawings, specifications, or other data are used for any purpose other than a definitely related Government procurement operation, the Government thereby incurs no responsibility nor any obligation whatsoever, and the fact that the Government may have formulated, furnished, or in any way supplied the said drawings, specifications, or other data is not to be regarded by implication or otherwise as in any manner licensing the holder or any other person or corporation or conveying any rights or permission to manufacture, use, or sell any patented invention that may in any way be related thereto.

This report has been reviewed by the Office of Information (OI) and is releasable to the National Technical Information Service (NTIS). At NTIS, it will be available to the general public, including foreign nations.

This technical report has been reviewed and is approved for publication.

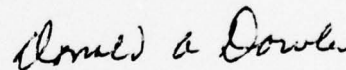


HOWARD G. HUDSON
Captain, USAF
Project Officer



J. PHILIP CASTILLO
Acting Chief, Technology Branch

FOR THE COMMANDER



DONALD A. DOWLER
Colonel, USAF
Chief, Electromagnetics Division

DO NOT RETURN THIS COPY. RETAIN OR DESTROY.

AD-E200 164

19 REPORT DOCUMENTATION PAGE		READ INSTRUCTIONS BEFORE COMPLETING FORM
1. REPORT NUMBER	2. GOVT ACCESSION NO.	3. RECIPIENT'S CATALOG NUMBER
(1) AFWL-TR-77-221	Vol 1 - VOL-1, V1	(9)
4. TITLE (and Subtitle)		5. TYPE OF REPORT & PERIOD COVERED
EXCITATION OF A WIRE IN A RECTANGULAR CAVITY.		Final Report.
Volume I: Theory.		6. PERFORMING ORG. REPORT NUMBER
7. AUTHOR(s)		8. CONTRACT OR GRANT NUMBER(s)
(10) D. B. Seidel		(15) ✓ AFOSR-76-3009 ✓
9. PERFORMING ORGANIZATION NAME AND ADDRESS		10. PROGRAM ELEMENT, PROJECT, TASK AREA & WORK UNIT NUMBERS
University of Arizona Tucson, Arizona 85724		(16) 64747F 12090525 (17) 45
11. CONTROLLING OFFICE NAME AND ADDRESS		12. REPORT DATE
Air Force Weapons Laboratory (ELT) Kirtland Air Force Base, NM 87117		(11) May 1978
14. MONITORING AGENCY NAME & ADDRESS (if different from Controlling Office)		13. NUMBER OF PAGES
Air Force Office of Scientific Research (NP) Bolling Air Force Base, Wash D C 20332		90
15. SECURITY CLASS. (of this report)		15a. DECLASSIFICATION/DOWNGRADING SCHEDULE
UNCLASSIFIED		
16. DISTRIBUTION STATEMENT (of this Report)		
(12) 98p. Approved for public release; distribution unlimited.		
17. DISTRIBUTION STATEMENT (of the abstract entered in Block 20, if different from Report)		
(18) AFWL, SBIE		
18. SUPPLEMENTARY NOTES		
19. KEY WORDS (Continue on reverse side if necessary and identify by block number)		
Rectangular Cavity Dyadic Green's Functions for Rectangular Cavity Small Aperture Wire Scatterer Shielding Effects		
20. ABSTRACT (Continue on reverse side if necessary and identify by block number) (UNCLASSIFIED)		
In this work, the problem of determining the currents excited on a wire enclosed within a rectangular cavity is considered. The wire and cavity interior are excited by electromagnetic sources exterior to the cavity which couple to the cavity interior through a small aperture in the cavity wall. It is assumed that the wire is thin, straight and oriented perpendicular to one of the cavity walls. An integral equation is formulated for the problem in the frequency domain using equivalent dipole moments to approximate the effects of the aperture. This integral equation is then solved numerically by the method of		

033 800

LB

next page

UNCLASSIFIED

SECURITY CLASSIFICATION OF THIS PAGE(When Data Entered)

moments. The dyadic Green's functions for this problem are difficult to compute numerically; consequently, extensive numerical analysis is necessary to render the solution tractable. Sample numerical results are presented for representative configurations of cavity, wire and aperture, and suggestions for future extensions of this work are discussed.

ADDITION for	
NTIS	White Section <input checked="" type="checkbox"/>
DDO	Bull Section <input type="checkbox"/>
UNANNOUNCED	<input type="checkbox"/>
JUSTIFICATION	
BY	
DISTRIBUTION/AVAILABILITY CODES	
Dist.	With a copy of SPECIAL
A	

UNCLASSIFIED

SECURITY CLASSIFICATION OF THIS PAGE(When Data Entered)

TABLE OF CONTENTS

	Page
LIST OF ILLUSTRATIONS	iii
LIST OF TABLES	v
1. INTRODUCTION	1
Modeling of the Physical Problem	1
Historical Background	2
2. FORMULATION	5
Dyadic Green's Functions	6
Integral Equation Formulation	12
Aperture Equivalent Dipole Moments	17
3. A PRELIMINARY TWO-DIMENSIONAL PROBLEM	27
Formulation	27
Reduction to Matrix Equation by Method of Moments	32
Numerical Considerations	36
Sample Calculations	40
Final Observations	47
4. NUMERICAL METHODS FOR CAVITY PROBLEM	49
Approximation by Matrix Equation	49
An Efficient Method of Computing the Sums Outside the Source Region	55
Numerical Evaluation of the Integral of the Singular Sum	59
Numerical Evaluation of the Deleted Green's Functions	67
5. NUMERICAL RESULTS FOR SAMPLE CASES	72
6. CONCLUSION	84
Suggested Extensions of this Work	85
LIST OF REFERENCES	88

LIST OF ILLUSTRATIONS

Figure	Page
1. Geometry for Aperture-Perforated Rectangular Cavity with Interior Wire	3
2. Equivalent Interior Problems	14
3. Small Aperture/Dipole Moment Equivalent Problems	18
4. Equivalent Interior Problem Which Accounts for Effects of Wall Reflections and Wire Currents on Aperture Dipoles . .	22
5. Geometry for Analogous Two-Dimensional Problem	28
6. Pulse Expansion Functions and Piecewise Sinusoidal Testing Functions for Two-Dimensional Problem	35
7. Aperture Field for Cavity with No Interior Wires	42
8. Aperture Field for Cavity with One Interior Wire	44
9. Aperture Field for Cavity with Two Interior Wires	45
10. Aperture Field for Cavity with One Interior Wire and $.4\lambda$ Aperture Width	46
11. Expansion and Testing Functions for Unknown Wire Currents .	51
12. Choice of Contours in m-n Plane for Efficient Summing of Double Series	58
13. Terms Used in Numerical Computation of Sums	58
14. Comparison of the Integrals of the Free Space Exact and Reduced Kernels	62
15. Example Computed Values of $\psi(z)$, $\psi_r(z)$ and $\psi_s(z)$	66
16. Example Computation for $G_{A_{zz}}$ and the Real Part of $\hat{G}_{A_{zz}}$. .	69
17. Example Computation of $g_{F_{yy}}$ and the Real Part of $\hat{g}_{F_{yy}}$. .	71

LIST OF ILLUSTRATIONS--Continued

Figure	Page
18. Currents Excited on $.2\lambda$ Wire for a $.2\lambda \times .25\lambda \times .3\lambda$ Cavity	73
19. Currents Excited on 1λ Wire in $.4\lambda \times .6\lambda \times 1.3\lambda$ Cavity . .	75
20. Currents Excited on $.5\lambda$ Wire for Slot Perpendicular and Parallel to \underline{z} Directed Incident Electric Field	77
21. Currents Excited on $.5\lambda$ Wire for Slot Perpendicular and Parallel to $\underline{-y}$ Directed Electric Field	79
22. Current Excited on $.55\lambda$ Wire Which Is Attached to Cavity Wall at One End	81
23. Current Excited on $.8\lambda$ Wire Which Is Attached to Cavity Wall at Both Ends	82

LIST OF TABLES

Table	Page
1. Dyadic Green's Functions for the Magnetic and Electric Vector Potentials	7
2. Dyadic Green's Functions for the Electric and Magnetic Fields Due to an Electric Current Source	9

CHAPTER 1

INTRODUCTION

An investigation of the problem of a wire inside a cavity which is excited by an external source has been undertaken. The effects of this external source are coupled to the cavity interior and wire through an aperture in the cavity wall. The currents excited upon the wire and the fields within the cavity are to be determined. This boundary value problem is an idealization of a wire in some metal enclosure. As examples, the wire may be inside the shielding or housing of an electronic or mechanical unit on an aircraft, or it might simply pass from one metal partition to another through a region which is essentially empty.

This paper deals primarily with the problem formulation (Chapter 2) and the consideration of the many numerical difficulties which are encountered in obtaining a solution (Chapter 4). In addition, an analogous two-dimensional problem is considered (Chapter 3) and some sample numerical results are given (Chapter 5). In Chapter 6, in addition to a summary of this work, several possible extensions are discussed. The remainder of this introductory chapter is devoted to the modeling of the problem and its historical background.

Modeling of the Physical Problem

In order to model the system of interest, a rectangular box having an aperture in a side wall and enclosing a wire is considered.

The appropriate geometry is shown in Figure 1. The problem is formulated in the frequency domain. It should be noted, however, that given the frequency domain solution, desired time domain quantities can be obtained by numerical inverse Fourier transform.

As is usual in the investigation of complex problems, simplifications must be invoked to render the problem tractable. The assumptions and conditions of the cavity/wire problem are summarized as follows:

1. The cavity is the interior region of a perfectly conducting rectangular box.
2. The material in the box is uniform, linear and isotropic.
3. The cavity is excited through a small aperture in a cavity wall such that aperture dipole approximations may be used.
4. The wire is straight, circular and perfectly conducting, and is oriented perpendicular to a side wall of the cavity.
5. The wire ends may or may not be in electrical contact with the cavity walls.
6. The wire is thin at the frequency of operation and thin-wire assumptions can be utilized.

Historical Background

In recent years, a great deal of work has been done on the problem of scattering from wires in free space and efficient techniques have been developed to handle them (Butler and Wilton 1975, Wilton and Butler 1976). More recently problems for which a wire couples to an aperture in an infinite planar screen have been considered (Lin, Curtis and Vincent 1976; Butler and Umashankar 1976; Seidel and Butler 1976).

Historically, the work done on the rectangular cavity problem has been primarily concerned with formulating the dyadic Green's

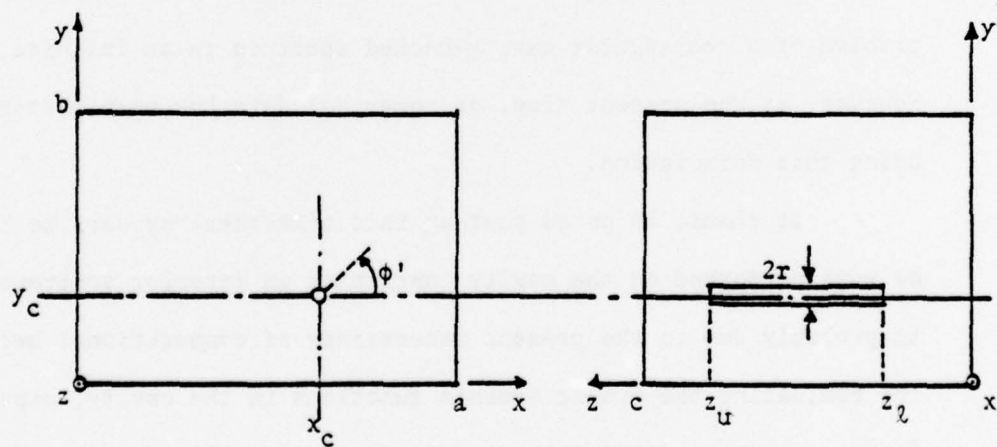
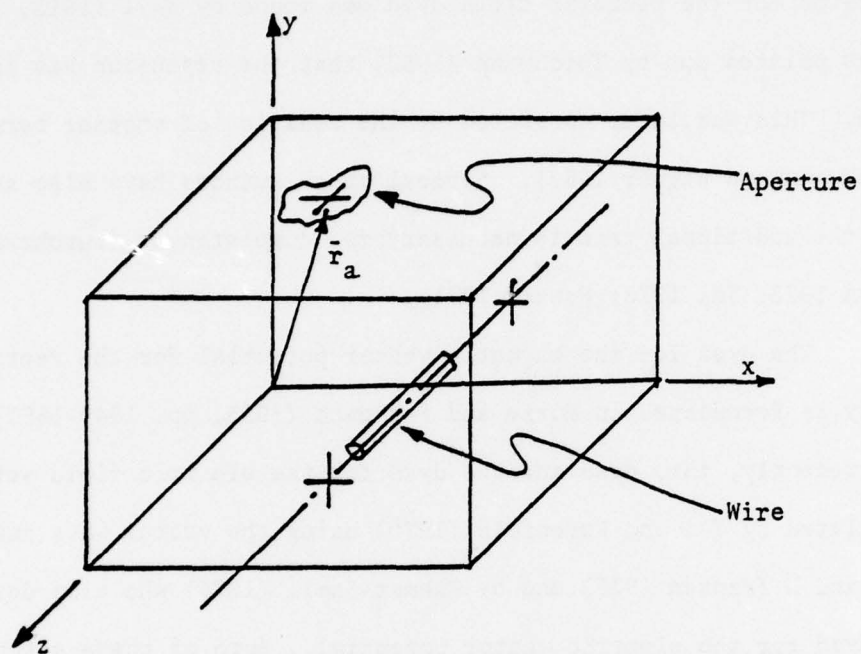


Figure 1. Geometry for Aperture-Perforated Rectangular Cavity with Interior Wire.

functions for the potentials and fields for a rectangular cavity. An expansion for the electric field dyad was found by Weyl (1913, 1915). It was pointed out by Teichmann (1952) that the expansion was incomplete. This was later corrected by the addition of another term (Teichmann and Wigner 1953). Several other authors have also shown that that the additional term is necessary for completeness (Kurokawa 1958; Collin 1973; Tai 1973; Howard 1974).

The dyad for the magnetic vector potential for the rectangular cavity is formulated in Morse and Feshbach (1953, pp. 1849-1851). More recently, this dyad and the dyad for the electric field were formulated by Tai and Rozenfeld (1976) using the vector wave functions \bar{L} , \bar{M} and \bar{N} (Hansen 1935) and by Rahmat-Samii (1975) who also derives the dyad for the electric vector potential. Both of these authors took care to insure completeness of the expansions.

Recently, Cheng and Chen (1976) formulated the solution for the problem of a rectangular cavity-backed aperture in an infinite screen. However, at the present time, no numerical data has been presented using this formulation.

It should be noted that at this time there appears to have been no work performed on the cavity containing an interior scatterer. This is probably due to the present uncertainty of computational methods for evaluating the dyadic Green's functions in the cavity, especially in or near source regions.

CHAPTER 2

FORMULATION

For the purposes of this problem, consider a perfectly conducting rectangular cavity. One corner of this cavity is located at the origin of a cartesian coordinate system (Figure 1). The dimensions of the cavity are denoted by a , b and c in the x , y and z directions, respectively. Within this cavity, there is a perfectly conducting, round thin wire of radius r ($r \ll \lambda$) which is parallel to the z -axis. This wire may or may not be attached to either or both walls of the cavity.

One of the walls of the cavity is perforated by a small aperture whose center is located at $\vec{r}_a = (x_a, y_a, z_a)$. The exterior region to which the aperture couples the cavity interior may be of two different types. The cavity may be located behind an infinite, perfectly conducting, planar screen such that the cavity wall containing the aperture is a portion of the infinite screen. Alternatively, the cavity may be situated in a free space environment. In either case, the excitation for the problem is provided by sources in the exterior region.

Finally, it is assumed that the medium in both the interior and exterior regions is homogeneous and isotropic and is characterized by (ϵ, μ) where ϵ can be complex for a lossy medium. It is assumed

that the problem is time harmonic with angular frequency ω and the factor $e^{j\omega t}$ has been suppressed throughout.

Dyadic Green's Functions

In order to formulate an integral equation for this problem, it is necessary to know the Green's functions for the potentials and the fields within the interior, or cavity, region. These Green's functions are dyadic in nature and, as one would expect, are singular in the source region.

One can define the dyadic Green's function for the magnetic vector potential by

$$(\nabla^2 + k^2) \bar{\bar{G}}_A(\vec{r}, \vec{r}') = -\bar{\bar{I}} \delta(\vec{r} - \vec{r}'), \quad (2.1a)$$

$$\hat{n} \times (k^2 \bar{\bar{I}} + \nabla \nabla) \cdot \bar{\bar{G}}_A = 0 \text{ on } S \quad (2.1b)$$

where k is the wavenumber of the homogeneous, isotropic medium of the cavity interior, $\bar{\bar{I}}$ is the identity dyad, \hat{n} is an inward-directed unit normal vector on S where S is the surface of the cavity. This Green's dyad has been derived by Tai and Rozenfeld (1976) in terms of the vector wave functions \bar{L} , \bar{M} and \bar{N} and is shown as a matrix in Table 1.

Once $\bar{\bar{G}}_A$ has been determined, the Green's dyads for the electric and magnetic fields due to an electric current source can be found. They are defined by

$$\bar{\bar{G}}_e = (k^2 \bar{\bar{I}} + \nabla \nabla) \cdot \bar{\bar{G}}_A \quad (2.2)$$

Table 1. Dyadic Green's Functions for the Magnetic and Electric Vector Potentials.

$$\bar{G}_A = \frac{1}{abc} \sum_{m,n,l=0}^{\infty} \frac{\epsilon_m \epsilon_n \epsilon_l}{K_{mnl}^2 - k^2} \left\{ \begin{array}{ccc} (cc)_x (ss)_y (ss)_z & 0 & 0 \\ 0 & (ss)_x (cc)_y (ss)_z & \\ 0 & 0 & (ss)_x (ss)_y (cc)_z \end{array} \right\}$$

$$\bar{G}_F = \frac{1}{abc} \sum_{m,n,l=0}^{\infty} \frac{\epsilon_m \epsilon_n \epsilon_l}{K_{mnl}^2 - k^2} \left\{ \begin{array}{ccc} (ss)_x (cc)_y (cc)_z & 0 & 0 \\ 0 & (cc)_x (ss)_y (cc)_z & 0 \\ 0 & 0 & (cc)_x (cc)_y (ss)_z \end{array} \right\}$$

where

$$(cc)_x (ss)_y (ss)_z = \cos k_x x \cos k_x x' \sin k_y y \sin k_y y' \sin k_z z \sin k_z z', \text{ etc.}$$

$$k_x = \frac{m\pi}{a}, k_y = \frac{n\pi}{b}, k_z = \frac{l\pi}{c}, K_{mnl}^2 = k_x^2 + k_y^2 + k_z^2$$

and

$$\epsilon_i = \begin{cases} 1, & i=0 \\ 2, & i \neq 0 \end{cases}$$

for the electric field and

$$\bar{\bar{G}}_h = \nabla \times \bar{\bar{G}}_A \quad (2.3)$$

for the magnetic field. The matrix forms of $\bar{\bar{G}}_e$ and $\bar{\bar{G}}_h$ are given in Table 2. They were obtained by simply operating upon $\bar{\bar{G}}_A$ as prescribed by (2.2) and (2.3).

It should be noted that this result for $\bar{\bar{G}}_e$ agrees with that derived by Tai and Rozenfeld (1976) directly using the vector wave functions. It also would agree with a similar result obtained by Rahmat-Samii (1975) if an obvious sign error in that paper were corrected. Note that this agreement is a most important point. In these two papers, the authors have taken great care to insure completeness of the expansion functions for $\bar{\bar{G}}_e$ in the source region of the cavity. The agreement between their results and that given here demonstrates the fact that completeness is insured when the problem is formulated through use of the potentials and the fields are then derived from those potentials.

It now remains to determine the dyadic Green's function for the electric vector potential and its related field dyads. Consider the Green's dyad for the electric vector potential defined by

$$(\nabla^2 + k^2) \bar{\bar{g}}_F(\vec{r}, \vec{r}') = - \bar{\bar{I}} \delta(\vec{r} - \vec{r}') \quad (2.4a)$$

$$\left. \begin{aligned} \hat{n} \cdot \bar{\bar{g}}_F &= 0 \\ \hat{n} \times \nabla \times \bar{\bar{g}}_F &= 0 \end{aligned} \right\}, \text{ on } S. \quad (2.4b)$$

Table 2. Dyadic Green's Functions for the Electric and Magnetic Fields Due to an Electric Current Source.

$$\begin{aligned} \bar{\bar{G}}_e &= \frac{1}{abc} \sum_{m,n,\ell=0}^{\infty} \frac{\epsilon_m \epsilon_n \epsilon_\ell}{K^2 mn\ell} - k^2 \begin{Bmatrix} (k^2 - k_x^2)(cc)_x(ss)_y(ss)_z - k_x k_y (cs)_x(sc)_y(ss)_z - k_x k_z (cs)_x(ss)_y(sc)_z \\ - k_x k_y (sc)_x(cs)_y(ss)_z (k^2 - k_y^2)(ss)_x(cc)_y(ss)_z - k_y k_z (ss)_x(cs)_y(sc)_z \\ - k_x k_z (sc)_x(ss)_y(cs)_z - k_y k_z (ss)_x(sc)_y(cs)_z (k^2 - k_z^2)(ss)_x(ss)_y(cc)_z \end{Bmatrix} \\ \bar{\bar{G}}_h &= \frac{1}{abc} \sum_{m,n,\ell=0}^{\infty} \frac{\epsilon_m \epsilon_n \epsilon_\ell}{K^2 mn\ell} - k^2 \begin{Bmatrix} 0 & -k_z(ss)_x(cc)_y(cs)_z & k_y(ss)_x(cs)_y(cc)_z \\ k_z(cc)_x(ss)_y(cs)_z & 0 & -k_x(cs)_x(ss)_y(cc)_z \\ -k_y(cc)_x(cs)_y(ss)_z & k_x(cs)_x(cc)_y(ss)_z & 0 \end{Bmatrix} \end{aligned}$$

where

$$(cs)_x(ss)_y(sc)_z = \cos k_x x \sin k_x x' \sin k_y y \sin k_y y' \sin k_z z \cos k_z z', \text{ etc.}$$

Rahmat-Samii (1975) has obtained a solution for \bar{g}_F . It is given in matrix form in Table 1. Again the sign error has been corrected.

Now that \bar{g}_F is determined, the dyads for the electric and magnetic fields due to a magnetic current source can be defined by

$$\bar{g}_e = - \nabla \times \bar{g}_F \quad (2.5)$$

and

$$\bar{g}_h = (k^2 \bar{I} + \nabla \nabla) \cdot \bar{g}_F \quad (2.6)$$

If \bar{g}_e is written in matrix form, it is found that

$$\bar{g}_e(\bar{r}, \bar{r}') = - \tilde{\bar{G}}_h(\bar{r}', \bar{r}) \quad (2.7)$$

where the tilde denotes the transpose of the dyad.

As a matter of notation, an upper case G denotes a dyad due to an electric current source; similarly a lower case g denotes a dyad due to a magnetic current source. The subscript A, F, e or h denotes the particular potential or field which is given by the dyad.

Before proceeding with the formulation of the integral equation, it is worthwhile to consider a few of the general properties of these dyadic Green's functions. Probably the most apparent property is that each component of each dyad is in itself a triply infinite Fourier sum. It can be seen, however, that any one of the sums can be performed analytically using one of the following relationships:

$$\sum_{m=1}^{\infty} \frac{1}{k_x^2 + \alpha^2} \sin k_x x \sin k_x x' = \frac{a}{2\alpha \sinh \alpha a} \sinh \alpha x_{<} \sinh \alpha (a - x_{>}) \quad (2.8a)$$

$$\sum_{m=0}^{\infty} \frac{\epsilon_m}{k_x^2 + \alpha^2} \cos k_x x \cos k_x x' = \frac{a}{\alpha \sinh \alpha a} \cosh \alpha x_{<} \cosh \alpha (a - x_{>}) \quad (2.8b)$$

$$\sum_{m=1}^{\infty} \frac{k_x}{k_x^2 + \alpha^2} \cos k_x x_{<} \sin k_x x_{>} = \frac{a}{2 \sinh \alpha a} \cosh \alpha x_{<} \sinh \alpha (a - x_{>}) \quad (2.8c)$$

$$\sum_{m=1}^{\infty} \frac{k_x}{k_x^2 + \alpha^2} \sin k_x x_{<} \cos k_x x_{>} = \frac{-a}{2 \sinh \alpha a} \sinh \alpha x_{<} \cosh \alpha (a - x_{>}) \quad (2.8d)$$

where

$$k_x = \frac{m\pi}{a}, \quad x_{<} = \min(x, x'), \quad x_{>} = \max(x, x'), \quad 0 \leq x, x' \leq a.$$

Equations (2.8) are easily derived by considering the ordinary differential equation

$$\left(\frac{d^2}{dx^2} + k_x^2 \right) g(x, x') = \delta(x - x')$$

on the interval $(0, a)$ with various combinations of unmixed Dirichlet and Neumann boundary conditions. The function g is then obtained by a closed form construction to obtain the right-hand side of (2.8) and also by a spectral expansion [to produce the left-hand side of (2.8)]. An alternative technique to derive these equations has been given by Collin (1960, p. 581).

Another important property of these triple sums can be seen if one remembers that both $\sinh x$ and $\cosh x$ approach $\pm \frac{1}{2} e^x$ for large x . Thus, if $|\bar{r}-\bar{r}'| \neq 0$, any one of the triple sums can be reduced to a double sum which is exponentially convergent. This demonstrates that outside the source region, all components of all the dyads converge, and in fact, converge exponentially. Therefore, all dyad components are uniformly convergent outside the source region (Titchmarsh 1939, p. 4).

Since it is valid to differentiate a series term by term provided the resulting series is uniformly convergent (Titchmarsh 1939, p. 37), the method used to construct the Green's dyads for the fields using (2.2), (2.3), (2.5) and (2.6) is valid outside the source region. This leads to the next observation regarding relative convergence of the sums. Note that the effect of a differential operator on each term of any one of the sums is to introduce a multiplicative factor of m , n , or l in the numerator. This will slow the rate of convergence of the series. Thus, for $|\bar{r}-\bar{r}'| \neq 0$, components of \bar{G}_A and \bar{g}_F will exhibit the most rapid convergence, whereas \bar{G}_e and \bar{g}_h , which are constructed using the second order differential operator $\nabla\nabla\cdot$, will exhibit the slowest convergence.

Integral Equation Formulation

To formulate the problem, one first uses the theories advanced for small apertures by Bethe (1944). This theory allows a small aperture, whose center is at the point \bar{r}_a , in a perfectly conducting screen to be replaced by equivalent electric and magnetic dipole moments

located at \bar{r}_a . Figure 2 (a and b) depicts this equivalence. The electric dipole moment \bar{P}_e is normal to the cavity wall, and the magnetic dipole moment \bar{P}_m is tangential to the cavity wall. Note that now the aperture has been shorted, and thus one has in this equivalent problem a wire scatterer in a rectangular cavity excited by the dipole sources \bar{P}_e and \bar{P}_m . (A more precise definition of these dipole moments will be considered later in this chapter.)

It is useful to make use of yet another equivalent problem. By using the equivalence principle (Harrington 1961) one can replace the wire scatterer in the cavity by unknown surface currents \bar{J}_s which are located upon a mathematical cylindrical surface which coincides with the surface of the wire in the original problem. This equivalence is shown in Figure 2 (b and c). Now one must force the boundary condition that the tangential electric field must vanish on the cylindrical surface. When this is accomplished the two problems are equivalent and the surface currents in the equivalent problem will be equal to the surface currents induced upon the wire in the original problem.

Note that in this second equivalent problem one has a cavity whose interior is entirely homogeneous and isotropic, and is driven by the unknown sources \bar{J}_s , \bar{P}_e and \bar{P}_m . Thus the fields in the cavity may be obtained by simply taking the scalar products of the appropriate dyadic Green's functions and these sources and integrating over the volume of the cavity.

The total electric field at the point \bar{r} in the cavity can be broken into two parts in the following manner:

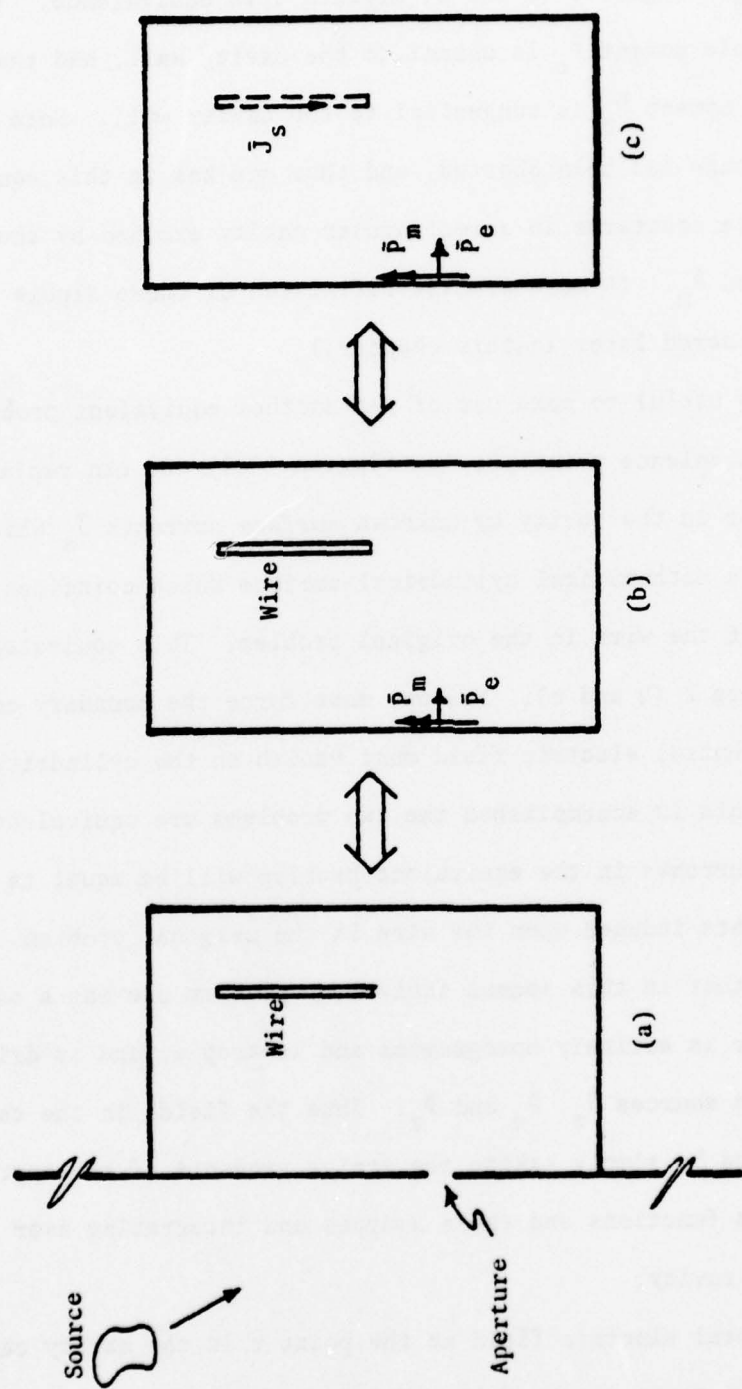


Figure 2. Equivalent Interior Problems.

$$\bar{E}(\bar{r}) = \bar{E}^i(\bar{r}) + \bar{E}^s(\bar{r}) \quad (2.9)$$

where \bar{E}^i is the field produced by the aperture dipole moments \bar{P}_e and \bar{P}_m and \bar{E}^s is the field produced by the surface current density \bar{J}_s .

Thus

$$\bar{E}^i(\bar{r}) = \frac{1}{\epsilon} \bar{G}_e(\bar{r}, \bar{r}_a) \cdot \bar{P}_e + jk\eta \bar{g}_e(\bar{r}, \bar{r}_a) \cdot \bar{P}_m \quad (2.10)$$

and

$$\bar{E}^s(\bar{r}) = -\frac{j\eta}{k} (k^2 \bar{I} + \nabla \nabla) \cdot \int \int_{\text{wire}} \bar{G}_A(\bar{r}, \bar{r}') \cdot \bar{J}_s(\bar{r}') d\bar{s}' \quad (2.11)$$

where $\eta = \sqrt{\mu/\epsilon}$ is the characteristic impedance of the medium interior to the cavity.

Since the wire scatterer is assumed to be thin ($r \ll \lambda$), one can use the traditional thin wire approximations to simplify (2.11). These approximations have been used extensively and are summarized as follows:

1. The circumferential component of current on the wire is negligible and may be assumed to vanish.
2. The remaining axial component of current has no circumferential variation.
3. There is no current on the end caps of the wire and the axial current must go to zero at the ends of the wire.
4. It is sufficient to require only the axial component of the electric field to vanish on the wire surface.

If these approximations are incorporated into (2.11), and the axial component of (2.9) is forced to vanish on the wire surface, one obtains the following integral equation:

$$\hat{w} \cdot \left[\frac{-j\eta}{k} (k^2 \bar{I} + \nabla \nabla) \cdot \int \int_{\text{wire}} \bar{G}_A(\bar{r}, \bar{r}') \cdot \hat{w} J_w(\bar{r}') ds' + \bar{E}^i(\bar{r}) \right] = 0 \quad (2.12)$$

where \bar{r} is on the wire surface and \hat{w} is a unit vector parallel to the axis of the wire.

It is seen that (2.12) is an integro-differential equation in which all three components of the dyadic kernel and all nine components of the dyadic operator $\nabla \nabla$ will, in general, couple. As will be seen in Chapter 4, the Green's functions are extremely difficult to calculate numerically in or near the source region. Because of this problem, the feasibility of solving (2.12) for the most general case of arbitrary wire orientation is questionable. However, if one considers the case where \hat{w} is equal to one of the three cartesian unit vectors (let that unit vector be \hat{z} by convention) then (2.12) reduces to a scalar integro-differential equation as follows:

$$\frac{-j\eta}{k} \left(\frac{d^2}{dz^2} + k^2 \right) \int \int_{\text{wire}} G_{A_{zz}}(\bar{r}, \bar{r}') J_z(z') ds' + \hat{z} \cdot \bar{E}^i(\bar{r}) = 0 \quad (2.13)$$

for \bar{r} on the wire surface.

Note that if (2.13) can be inverted, a solution for J_z will be obtained. However it should be remembered that \bar{E}^i contains \bar{P}_e and \bar{P}_m , which as of yet are unknown. Thus it remains to obtain additional constraints which will uniquely specify the values of these dipole moments.

Aperture Equivalent Dipole Moments

Before attempting to determine the dipole moments \bar{P}_e and \bar{P}_m , it is necessary to review the basis of small aperture theory. This summary is patterned after that in a recent paper by Butler (1976) and the work of Collin (1960). Consider an infinite perfectly conducting screen at $z = 0$ which separates two half spaces of the same properties (μ, ϵ). This screen is perforated by a small aperture centered about the point $(0,0,0)$. If the aperture is sufficiently small and \bar{r} is sufficiently far from the aperture, then the fields at \bar{r} due to the aperture can be approximated by the radiation from an electric dipole with moment \bar{P}_e and a magnetic dipole with moment \bar{P}_m located at $(0,0,0)$ which radiate in the presence of the unperforated screen. This equivalence is illustrated in Figure 3.

The moments of the electric and magnetic dipoles for the right half-space ($z > 0$), which are located at $(0,0,0+)$ are given by

$$\bar{P}_e = \epsilon \alpha_e (E_z^{sc-}(\bar{0}) - E_z^{sc+}(\bar{0})) \hat{z} \quad (2.14a)$$

and

$$\bar{P}_m = - \bar{\alpha}_m \cdot (\bar{H}^{sc-}(\bar{0}) - \bar{H}^{sc+}(\bar{0})) \quad (2.14b)$$

where $(\bar{E}^{sc-}, \bar{H}^{sc-})$ are the short circuit fields in the left half-space, that is, the fields in left half-space in the presence of the unperforated screen. Similarly, $(\bar{E}^{sc+}, \bar{H}^{sc+})$ are the short circuit fields in

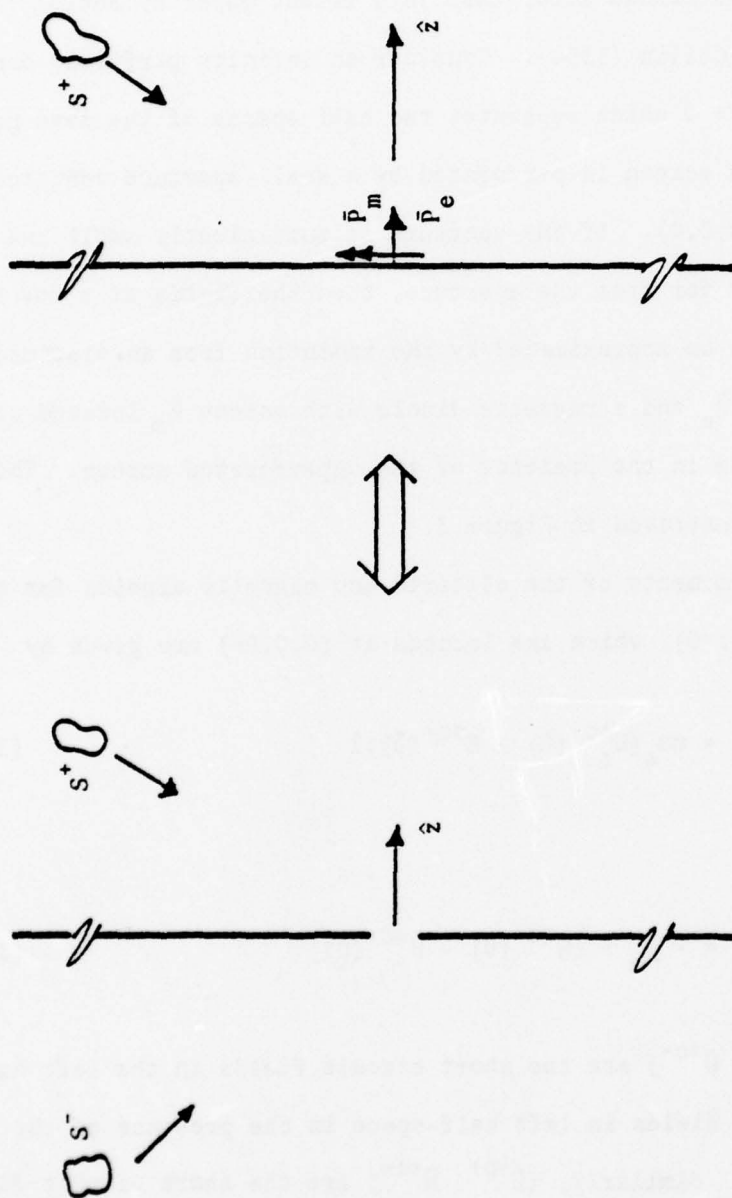


Figure 3. Small Aperture/Dipole Moment Equivalent Problems.

the right half-space. The electric polarizability α_e and the magnetic polarizability $\bar{\alpha}_m$ relate the specific excitation to the moments for a given aperture. Polarizabilities are available in the literature (Bouwkamp 1954; DeMeulenaere and Van Bladel 1977; Collin 1960, pp. 285-302; Cohn 1951, 1952) for several small apertures. Specifically, for an elliptical aperture defined by $(x^2/\ell^2) + (y^2/w^2) = 1$ for $\ell \geq w$,

$$\alpha_e = \frac{\pi w^2 \ell}{3E(\xi)}, \quad (2.15a)$$

$$\alpha_{m_{xx}} = \frac{1}{3} \frac{\pi \ell^3 \xi}{K(\xi) - E(\xi)}, \quad (2.15b)$$

$$\alpha_{m_{yy}} = \frac{1}{3} \frac{\pi \ell^3 \xi}{\left(\frac{\ell}{w}\right)^2 E(\xi) - K(\xi)}, \quad (2.15c)$$

and all other components of $\bar{\alpha}_m$ are zero. The square of the eccentricity (ξ) is defined by

$$\xi = 1 - \left(\frac{w}{\ell}\right)^2$$

and K and E are the complete elliptic integrals of the first and second kind, respectively, as defined by Abramowitz and Stegun (1965, p. 590).

It should be noted that, where the small aperture theory is based upon an aperture coupling two half-spaces, in the actual problem of interest the interior region is a rectangular cavity and the exterior region may or may not be a half-space.

First, consider the exterior region. Suppose the cavity is behind an infinite screen, such that the exterior region is actually a half-space. Then the short circuit exterior fields are easily determined from a knowledge of the incident field by application of physical optics.

However, if the cavity is not behind a perfectly conducting screen, the problem becomes more difficult. It now becomes necessary to determine the short circuit fields on the exterior surface of a rectangular box scatterer. This problem has been solved numerically by Tsai, Dudley and Wilton (1974). Since the short circuit fields are related to the surface current and charge by

$$\vec{J}_s = \hat{n} \times \vec{H}^{SC-}$$

and

$$q_s = \epsilon \hat{n} \cdot \vec{E}^{SC-},$$

these values could also be provided by experimental measurements of surface charge and current densities. Note that $(\vec{E}^{SC-}, \vec{H}^{SC-})$ and $(\vec{E}^{SC+}, \vec{H}^{SC+})$ have been defined for the problem of interest to be the short circuit fields in the exterior and interior regions, respectively. For the remainder of this paper it will be assumed that $(\vec{E}^{SC-}, \vec{H}^{SC-})$ are known.

Now consider the interior region of the problem as illustrated in Figure 2c. It is readily seen that $(\vec{E}^{SC+}, \vec{H}^{SC+})$ will be driven by the surface currents on the wire. However, this region is a cavity,

and the use of yet another equivalent problem is necessary in order to account for this problem properly. If the method of images (Collin 1960) is applied to the equivalent problem depicted by Figure 2c, a new equivalent problem can be obtained in which the aperture dipoles and the wire currents have been imaged in such a way that there is a three-dimensional infinite array of image sources in a half-space. A two-dimensional cross-section of that array is given in Figure 4. This means that $(\vec{E}^{sc+}, \vec{H}^{sc+})$ are produced by all of the sources in that half-space except for the original aperture dipoles \vec{P}_e and \vec{P}_m located at \vec{r}_a .

Now if it is realized that these arrays of image sources in the half-space are equivalent to the original sources in the cavity (the problem of Figure 2c), one obtains the following relations for the short circuit fields in the cavity region:

$$\begin{aligned} \vec{E}_n^{sc+}(\vec{r}) = & \hat{G}_{e_{nn}}(\vec{r}, \vec{r}_a) \vec{P}_{e_n} + jk\eta \hat{n} \cdot \hat{g}_e(\vec{r}, \vec{r}_a) \cdot \vec{P}_m \\ & - \frac{j\eta}{k} \iint_{\text{wire}} \vec{G}_{e_{nz}}(\vec{r}, \vec{r}') J_z(\vec{r}') ds' \end{aligned} \quad (2.16a)$$

and

$$\begin{aligned} \vec{H}^{sc+}(\vec{r}) = & \frac{jk}{\eta} \hat{G}_h(\vec{r}, \vec{r}_a) \cdot \hat{n} \vec{P}_{e_n} + \hat{g}_h(\vec{r}, \vec{r}_a) \cdot \vec{P}_m \\ & + \iint_{\text{wire}} \vec{G}_h(\vec{r}, \vec{r}') \cdot \hat{z} J_z(\vec{r}') ds' \end{aligned} \quad (2.16b)$$

where \hat{n} is the unit vector in the wall of the aperture and the symbol $(\hat{})$ over the dyads indicates that the original or self term of the image series (Green's function for half-space) has been deleted. Thus

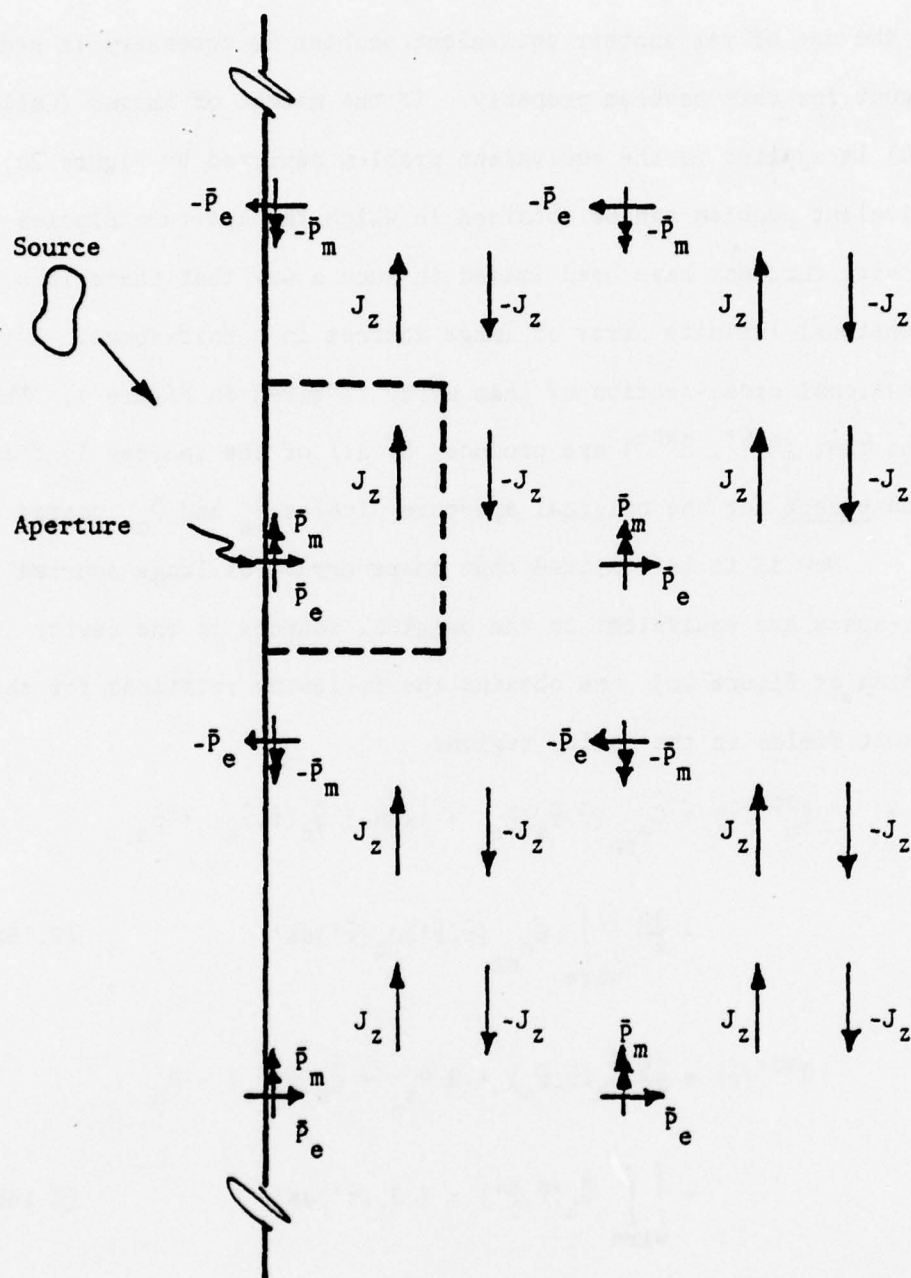


Figure 4. Equivalent Interior Problem Which Accounts for Effects of Wall Reflections and Wire Currents on Aperture Dipoles.

$$\hat{\bar{G}}_A(\bar{r}, \bar{r}_a) = \bar{G}_A(\bar{r}, \bar{r}_a) - \bar{I} \frac{e^{-jkR}}{2\pi R} \quad (2.17a)$$

and

$$\hat{\bar{g}}_F(\bar{r}, \bar{r}_a) = \bar{g}_F(\bar{r}, \bar{r}_a) - \bar{I} \frac{e^{-jkR}}{2\pi R} \quad (2.17b)$$

where $R = |\bar{r} - \bar{r}_a|$. Now the desired dyads may be obtained using the following relations:

$$\hat{\bar{G}}_e = (k^2 \bar{I} + \nabla \nabla) \cdot \hat{\bar{G}}_A, \quad (2.18a)$$

$$\hat{\bar{G}}_h = \nabla \times \hat{\bar{G}}_A, \quad (2.18b)$$

$$\hat{\bar{g}}_e = -\nabla \times \hat{\bar{g}}_F, \quad (2.18c)$$

and

$$\hat{\bar{g}}_h = (k^2 \bar{I} + \nabla \nabla) \cdot \hat{\bar{g}}_F. \quad (2.18d)$$

The functions defined by (2.17) and (2.18) will be referred to as deleted Green's functions in an effort to indicate the deletion of the singular, free space Green's function.

One now defines \hat{a}_1 and \hat{a}_2 to be the two cartesian unit vectors which are tangential to the wall of the aperture in such a fashion that $\hat{a}_1 \times \hat{a}_2 = \hat{n}$. For example, if the aperture were in the $y = 0$ wall of the cavity, then \hat{a}_1 would be \hat{z} , \hat{a}_2 would be \hat{x} and \hat{n} would be \hat{y} .

Note that since \bar{P}_e has only a normal component and \bar{P}_m has only a tangential component, there are only three non-vanishing unknowns: P_{e_n} , P_{m_1} and P_{m_2} . If new unknowns E_{T_n} and \bar{H}_T are introduced such that

$$E_{T_n} = E_n^{SC-}(\bar{r}_a) - E_n^{SC+}(\bar{r}_a) \quad (2.19a)$$

and

$$\bar{H}_T = \bar{H}^{SC-}(\bar{r}_a) - \bar{H}^{SC+}(\bar{r}_a) \quad (2.19b)$$

then by (2.14)

$$\frac{P_{e_n}}{\epsilon} = \alpha_e E_{T_n}, \quad (2.20a)$$

$$P_{m_1} = -\alpha_{m_{11}} H_{T_1} \quad (2.20b)$$

and

$$P_{m_2} = -\alpha_{m_{22}} H_{T_2}. \quad (2.20c)$$

Now, if (2.20) is substituted into (2.16), which in turn is substituted into (2.19) one obtains the following equations:

$$\begin{aligned}
& [1 + \alpha_e \hat{G}_{enn}(\bar{r}_a, \bar{r}_a)] E_{T_n} - jk\eta [\alpha_{m11} \hat{g}_{en1}(\bar{r}_a, \bar{r}_a) H_{T_1} + \alpha_{m22} \hat{g}_{en2}(\bar{r}_a, \bar{r}_a) H_{T_2}] \\
& - \frac{j\eta}{k} \int \int_{\text{wire}} G_{enz}(\bar{r}_a, \bar{r}') J_z(\bar{r}') ds' = E_n^{\text{sc-}}(\bar{r}_a) , \quad (2.21a)
\end{aligned}$$

$$\begin{aligned}
& \frac{jk}{\eta} \alpha_e \hat{G}_{h1n}(\bar{r}_a, \bar{r}_a) E_{T_n} + [1 - \alpha_{m11} \hat{g}_{h11}(\bar{r}_a, \bar{r}_a)] H_{T_1} - \alpha_{m22} \hat{g}_{h12}(\bar{r}_a, \bar{r}_a) H_{T_2} \\
& + \int \int_{\text{wire}} G_{h1z}(\bar{r}_a, \bar{r}') J_z(\bar{r}') ds' = H_1^{\text{sc-}}(\bar{r}_a) , \quad (2.21b)
\end{aligned}$$

$$\begin{aligned}
& \frac{jk}{\eta} \alpha_e \hat{G}_{h2n}(\bar{r}_a, \bar{r}_a) E_{T_n} - \alpha_{m11} \hat{g}_{h21}(\bar{r}_a, \bar{r}_a) H_{T_1} + [1 - \alpha_{m22} \hat{g}_{h22}(\bar{r}_a, \bar{r}_a)] H_{T_2} \\
& + \int \int_{\text{wire}} G_{h2z}(\bar{r}_a, \bar{r}') J_z(\bar{r}') ds' = H_2^{\text{sc-}}(\bar{r}_a) . \quad (2.21c)
\end{aligned}$$

It should be noted that the unknowns E_{T_n} , H_{T_1} and H_{T_2} are related to the unknown dipole moments by the aperture polarizabilities. Thus if (2.20) is substituted into (2.10) one obtains

$$\begin{aligned}
\hat{z} \cdot E^i(\bar{r}) &= \alpha_e G_{enz}(\bar{r}, \bar{r}_a) E_{T_n} - jk\eta \alpha_{m11} g_{ez1}(\bar{r}, \bar{r}_a) H_{T_1} \\
&- jk\eta \alpha_{m22} g_{ez2}(\bar{r}, \bar{r}_a) H_{T_2} \quad (2.22)
\end{aligned}$$

This means that (2.13) contains the unknowns E_{T_n} , H_{T_1} and H_{T_2} in addition to J_z . The three additional constraints provided by (2.21)

when solved simultaneously with (2.13) will provide a unique solution for the currents on the wire and the quantities E_{T_n} , H_{T_1} and H_{T_2} .

It is helpful at this point to attempt to describe physically the various terms in (2.21). First, it is noted that the terms containing the deleted Green's functions account for the fact that the aperture dipoles will be affected by the fields reflected back from the cavity walls. This is apparent if it is remembered that these terms are the fields in the aperture due to the array of the images of the aperture dipole. These virtual sources account for all of the reflections and multiple reflections from the cavity walls.

It can also be noted that the integral term in (2.21) represents the field scattered back into the aperture by the wire and thus accounts for the coupling between the currents on the wire and the aperture dipoles. If all of these coupling effects are assumed to be negligible, (2.21) reduces to $(E_{T_n}, \bar{H}_T) = (E_n^{sc-}, \bar{H}^{sc-})$. If on the other hand these effects are not neglected, the difference between (E_{T_n}, \bar{H}_T) and $(E_n^{sc-}, \bar{H}^{sc-})$ will in some way reflect the degree of to which the cavity walls and the wire scatterer couple to the aperture.

CHAPTER 3

A PRELIMINARY TWO-DIMENSIONAL PROBLEM

In an effort to gain insight for the three-dimensional cavity problem, it is helpful to consider an approximately analogous two-dimensional problem. For this case, the kernel functions would also be singular Fourier series, although of lower dimensionality. Thus where in the original problem the sums were doubly and triply-infinite, they are one- and two-dimensional in this two-dimensional analog. In addition to any insights which this effort might provide toward the solution of the three-dimensional cavity, the solution to this analogous problem may provide data pertinent to the physical problem being modeled. For example, in this simpler model, it is feasible to account for the actual coupling through a large aperture rather than use the aperture dipoles for small apertures.

Formulation

The geometry of the analogous problem is shown in Figure 5. It consists of an incident plane wave impinging upon a perfectly conducting infinite planar screen perforated by an infinite z-directed slot of width d . The slot is backed by a rectangular cylindrical cavity of depth a and width b . Within the cavity are L z-directed thin wires of various radii. The incident plane wave is polarized such that \vec{E} is parallel to the slot. Thus only the E_z , H_x and H_y field components are excited.

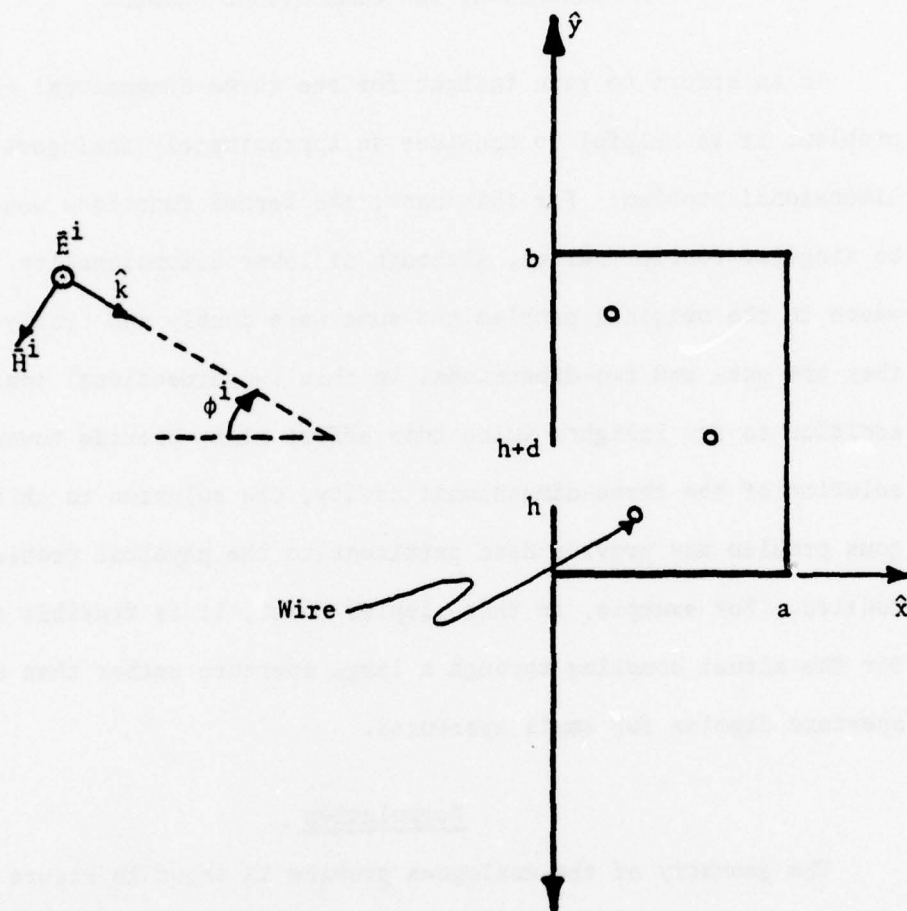


Figure 5. Geometry for Analogous Two-Dimensional Problem.

One now formulates the problem, using the thin wire approximations described previously in Chapter 2, by expressing E_z and H_y in terms of the unknown aperture electric field and the unknown surface currents on the wires. Then by forcing the boundary conditions that E_z and H_y be continuous through the aperture and E_z vanish on the wire surfaces, two coupled integral equations are obtained. They are

$$\begin{aligned} & \frac{1}{2k\eta} \left(\frac{d^2}{dy^2} + k^2 \right) \int_h^{h+d} E_z^a(y') [H_0^{(2)}(k|y-y'|) + jS_1(y,y')] dy' \\ & + \sum_{\ell=1}^L J_\ell \int_{\ell\text{th wire}} S_2(x',y,y') dc' \\ & = -2 H_y^{\text{inc}}(0,y), \quad h < y < h+d \end{aligned} \quad (3.1a)$$

and

$$\begin{aligned} & \int_h^{h+d} E_z^a(y') S_2(x,y,y') dy' \\ & - jk\eta \sum_{\ell=1}^L J_\ell \int_{\ell\text{th wire}} S_3(x,x',y,y') dc' \\ & = 0, \quad (x,y) \text{ on surface of the } s\text{th wire, for } s = 1, 2, \dots, L \end{aligned} \quad (3.1b)$$

where E_z^a is the unknown aperture electric field, J_ℓ is the surface current density on the ℓ th wire, H_y^{inc} is the y-component of the incident magnetic field and $\eta = \sqrt{\mu/\epsilon}$ is the characteristic impedance of the space. The functions S_1 , S_2 , and S_3 are defined by

$$S_1(y, y') = \frac{2}{ab} \sum_{m,n=0}^{\infty} \frac{\epsilon_m}{K_{mn}^2 - k^2} \text{sinc}_{y,y'} \quad (3.2a)$$

$$S_2(x, y, y') = \frac{4}{ab} \sum_{m,n=1}^{\infty} \frac{k_x}{K_{mn}^2 - k^2} \text{sinc}_x \text{sinc}_y \text{sinc}_{y'} \quad (3.2b)$$

and

$$S_3(x, x', y, y') = \frac{4}{ab} \sum_{m,n=1}^{\infty} \frac{1}{K_{mn}^2 - k^2} \text{sinc}_x \text{sinc}_{x'} \text{sinc}_y \text{sinc}_{y'} \quad (3.2c)$$

where $K_{mn}^2 = k_x^2 + k_y^2$, $k_x = \frac{m\pi}{a}$ and $k_y = \frac{n\pi}{b}$.

Note that any of the double sums in (3.2) can be reduced to a single sum by use of (2.8) and will thus converge exponentially as long as $\vec{r} \neq \vec{r}'$ [that is, when $(x, y) \neq (x', y')$].

Now assume that no two wires touch one another and that no wire is in the aperture region. This means then that with the exception of the first sum all of the infinite sums in (3.1a) are uniformly convergent. Indeed this first sum is uniformly convergent everywhere except when $y = y'$ in which case it diverges like $\sum \frac{1}{n}$. Similarly, all

sums in (3.1b) are uniformly convergent, with the exception of the term where $l=s$, in which case one point on the surface of integration will coincide with the point (x,y) .

It is now useful to make the approximation that the wire current resides at the center of the wire and that field boundary conditions are still enforced at the wire surface. This approximation is commonly known as the reduced kernel approximation. For this problem it can be stated by

$$\int_{\text{wire}} S_3(x,x',y,y')dc' \approx 2\pi r S_3(x,x_c,y,y_c) \quad (3.3)$$

where (x_c,y_c) is the center point of the wire and r is the wire radius. This can be justified by noting that S_3 , the Green's function for the magnetic vector potential in the cavity, must contain the free space two-dimensional Green's function, which goes as $\ln|\bar{r}-\bar{r}'|$. Note that $\ln|\bar{r}-\bar{r}'|$ can be integrated analytically over the wire surface, where \bar{r} is also on the wire surface, to give the desired result that

$$\int_{-\pi}^{\pi} \ln(2r \sin \frac{|\phi'|}{2}) r d\phi' = 2\pi r \ln r .$$

Since the wire is thin and the remaining portion of S_3 is a smooth, homogeneous solution to the wave equation, it too can be validly approximated by this technique. It should be noted that given the wire radii small but finite, the application of the reduced kernel approximation makes all of the infinite sums in (3.1b) uniformly convergent.

Reduction to Matrix Equation by Method of Moments

An effective technique for the numerical solution of integral equations in electromagnetics is the method of moments (Harrington 1968). Consider the operator equation

$$L\bar{u} = \bar{f} \quad (3.4)$$

where L is a linear operator, \bar{f} is a known vector, and \bar{u} is an unknown vector for which the solution is desired. Using the method of moments, one approximates \bar{u} by a finite linear combination of expansion vectors \bar{u}_n . Thus let

$$\bar{u} = \sum_{q=1}^N a_q \bar{u}_q \quad (3.5)$$

Now take the inner product of (3.4) with N testing vectors \bar{w}_p . If (3.5) is substituted into this result, and it is noted that L is linear, one arrives at the matrix equation

$$\sum_{q=1}^N \langle \bar{w}_p, L\bar{u}_q \rangle a_q = \langle \bar{w}_p, \bar{f} \rangle, \quad p = 1, 2, 3, \dots, N \quad (3.6)$$

Note that (3.1a) is a linear operator equation with an integro-differential operator and unknown function $E_z^a(y)$ and the unknowns $\{J_n\}$. Further, one has the boundary condition that E_z^a must vanish at each edge of the aperture because the tangential electric field (E_z) must vanish at these two points. If the inner product for this space is defined to be

$$\langle u, v \rangle = \int_h^{h+d} u(y)v(y)dy$$

the method of moments may be applied to approximate (3.1a) by a matrix equation.

The optimum choice of expansion functions (\bar{u}_p) and testing functions (\bar{w}_p) for this integro-differential operator and these boundary conditions has been the subject of many examinations (Butler and Wilton 1975; Wilton and Butler 1976). It has been shown that one efficient choice (Wilton and Butler 1976) is that of pulse, or piecewise-constant, expansion functions and piecewise-sinusoidal testing functions, denoted p_q and Λ_p^s respectively and defined in the coordinate system of this problem by

$$p_q(y) = \begin{cases} 1, & |y-y_q| < \frac{\Delta}{2} \\ 0, & |y-y_q| > \frac{\Delta}{2} \end{cases} \quad (3.7)$$

and

$$\Lambda_p^s(y) = \begin{cases} \text{sinc}(\Delta - |y-y_p|), & |y-y_p| < \Delta \\ 0, & |y-y_p| > \Delta \end{cases} \quad (3.8)$$

where $\Delta = d/(N+1)$ and $y_q = h+q\Delta$. Thus the unknown aperture field is approximated by

$$E_z^a(y) = \sum_{q=1}^N E_q p_q(y). \quad (3.9)$$

Figure 6 shows a plot of such an approximation as well as the testing functions $\Lambda_p^s(y)$. It should be noted that a half-pulse of zero amplitude has been placed at each end of the aperture. This is done because of the boundary condition that E_z^a vanish at each end of the aperture.

In order to perform the inner product one takes advantage of the piecewise-sinusoidal testing functions and the differential portion of the operator, $\frac{d^2}{dy^2} + k^2$, and integrates by parts twice. The integral portion of the result vanishes, leaving only three boundary terms.

If these expansion and test functions are applied to (3.1a) and the same expansion functions are substituted into (3.1b), the following equations are obtained

$$\begin{aligned} \frac{1}{2\eta} \sum_{q=1}^N E_q [F_q(y_{p-1}) - 2\cos k\Delta F_q(y_p) + F_q(y_{p+1})] \\ + C \sum_{\ell=1}^L I_{\ell} S_2(x_{\ell}, y_p, y_{\ell}) = - 2CH_y^{\text{inc}}(0, y_p) \end{aligned} \quad (3.10a)$$

for $p = 1, 2, \dots, N$ and

$$\sum_{q=1}^N E_q \int_{\Delta q} S_2(x_s, y_s, y') dy' - jk\eta \sum_{\ell=1}^L I_{\ell} S_3(x_s, x_{\ell}, y_s, y_{\ell}) = 0 \quad (3.10b)$$

for $s = 1, 2, \dots, L$ where

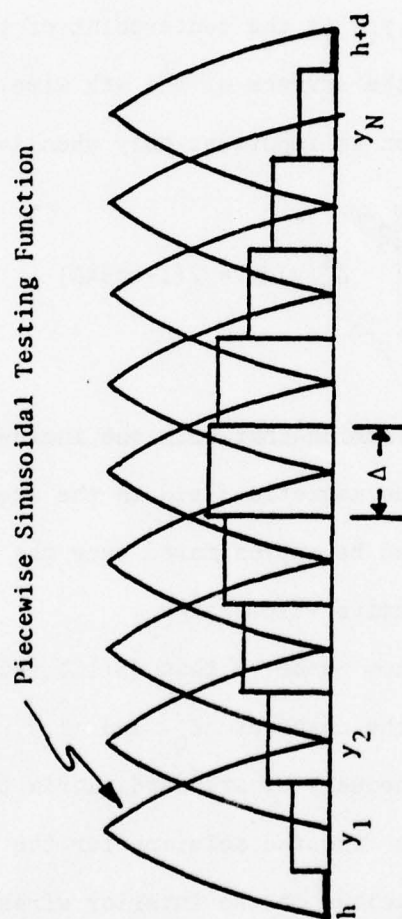


Figure 6. Pulse Expansion Functions and Piecewise Sinusoidal Testing Functions for Two-Dimensional Problem.

$$F_q(y) = \int_{\Delta q} H_0^{(2)}(k|y-y'|) dy' + j \int_{\Delta q} S_1(y, y') dy' \quad (3.11)$$

In (3.10), $I_\ell = 2\pi r_\ell J_\ell$ is the current due to the uniform surface current density on the ℓ th wire and Δq is the interval $(y_q - \frac{\Delta}{2}, y_q + \frac{\Delta}{2})$. The point $\bar{r}_\ell = (x_\ell, y_\ell)$ is the centerpoint of the ℓ th wire and $\bar{r}_s = (x_s, y_s)$ is a point on the surface of the s th wire. However, for thin wires, this distinction is important only when $\ell=s$. The constant

$$C = \int_{y_p - \Delta}^{y_p + \Delta} \Lambda_p^s(y) dy = 2(1 - \cos k\Delta)$$

results from assuming that both the incident magnetic field at the aperture and the magnetic field in the aperture excited by the currents on the wires can be approximated over the range of p th testing function by their respective values at y_p .

It is now observed that (3.10) represents two coupled matrix equations for the unknowns $\{E_q\}$ and $\{I_\ell\}$. These equations can be solved simultaneously by standard matrix techniques, such as Gauss elimination, to find the solution for the unknown aperture field and the currents excited on the interior wires.

Numerical Considerations

Although the problem has been formulated and the integral equations have been approximated by matrix equation (3.10), it is noted

that one must be able to calculate the infinite sums S_2 and S_3 , possibly near the source where convergence is poor. The sums S_1 and S_2 must be integrated, S_1 over the source region (3.11). Consequently, it becomes necessary to develop techniques for handling these situations.

First it should be noted that in (3.10b) it is valid to integrate S_2 term by term since S_2 will always be uniformly convergent over the range of the integration (Titchmarsh 1939, p. 36). It can be shown that S_1 in (3.11) can also be integrated term by term, even though at $y=y'$, S_1 diverges. Because S_1 is uniformly convergent at every other point in the range of integration, and because the series that results if S_1 is integrated term by term is absolutely convergent, it is valid to integrate S_1 term by term (Titchmarsh 1939, pp. 44-45). This is an important result since as a general rule it is numerically more efficient to integrate the series term by term.

It remains to develop a technique for efficiently summing these series, even when $|\vec{r}-\vec{r}'|$ is small. It is expected that the convergence will be poor from a numerical standpoint. To demonstrate the method which is used to make this improvement, consider the special case of S_3 (3.2c). By applying (2.8a) to (3.2c) one finds that

$$S_3 = \frac{2}{a} \sum_{m=1}^{\infty} \text{sink}_x x \text{ sink}_x x' \frac{\sinh \gamma_b y_< \sinh \gamma_b (b-y_>)}{\gamma_b \sinh \gamma_b b} \quad (3.12)$$

where $\gamma_b^2 = k_x^2 - k^2$.

Note that just as easily the double sum could have been reduced by eliminating the sum over m . Thus, there is always a choice of which sum to remove analytically by (2.8). Let S_3^{asy} be defined as the asymptotic series of S_3 such that its terms are the limit of the terms in (3.12) for large m . Thus

$$S_3^{\text{asy}} = \frac{1}{\pi} \sum_{m=1}^{\infty} \frac{1}{m} \sin m\pi \frac{x}{a} \sin \frac{m\pi x'}{a} e^{-m\pi \frac{|y-y'|}{a}}. \quad (3.13)$$

Series S_3 has exponential convergence, the rapidity of which increases as $|y-y'|/a$ increases. It can easily be seen that if the sum over m were removed analytically, S_3 would converge exponentially like $|x-x'|/b$. It is reasonable to assume from this that as a general rule $|y-y'|/a$ should be compared to $|x-x'|/b$ and (3.2) should be reduced to a single sum in that way which maximizes this exponential convergence. For example, if $|y-y'|/a > |x-x'|/b$, then (3.2c) should be reduced to (3.12). Indeed, the validity of this general rule can be substantiated by the results of numerical testing.

Now return to (3.12). Suppose, however, that although $|y-y'|/a$ is larger than $|x-x'|/b$, it too is small, and (3.12) remains poorly convergent. Convergence of such a series can often be greatly improved if a closed form expression can be found for the corresponding asymptotic series (Lewin 1975). This means that if $S = \sum_n s_n$, $s_n \rightarrow s_n'$ as $n \rightarrow \infty$, and $S' = \sum_n s_n' = h$ where h is a closed form expression, then $D = \sum_n (s_n - s_n')$ will converge more rapidly than S . Consequently, S

can be evaluated by $S = h + D$. Thus if (3.13) can be evaluated in closed form, the convergence of (3.12) could be improved.

For this particular sum, S_3 , one rewrites (3.13) as

$$S_3^{\text{asy}} = \frac{1}{2\pi} \sum_{m=1}^{\infty} \frac{e^{-m\alpha}}{m} (\cos m\beta_1 - \cos m\beta_2) \quad (3.14)$$

where

$$\alpha = \frac{\pi|y-y'|}{a}, \quad \beta_1 = \frac{\pi|x-x'|}{a} \quad \text{and} \quad \beta_2 = \frac{\pi(x+x')}{a}.$$

But it is known that (Jolley 1961, pp. 110-111)

$$\sum_{n=1}^{\infty} \frac{e^{-nx}}{n} \cos n\lambda = \frac{x}{2} - \frac{1}{2} \ln(\cosh x - \cos \lambda) - \frac{1}{2} \ln 2. \quad (3.15)$$

With the use of (3.14) and (3.15), (3.12) becomes

$$S_3 = \frac{2}{a} \sum_{m=1}^{\infty} \text{sink}_x x \text{ sink}_x x' \left[\frac{\sinh \gamma_b y_< \sinh \gamma_b (b-y_>)}{\gamma_b \sinh \gamma_b b} - \frac{1}{2} \frac{e^{-m\alpha}}{k_x} \right] + \frac{1}{4\pi} \ln \left(\frac{\cosh \alpha - \cos \beta_2}{\cosh \alpha - \cos \beta_1} \right). \quad (3.16)$$

It should be noted that numerically the sum in (3.16) is rapidly convergent regardless of how small $|\bar{r}-\bar{r}'|$ is, so long as it is not zero. Indeed at $|\bar{r}-\bar{r}'| = 0$, α and β_1 go to zero and from (3.16) it is seen that S_3 possesses the expected logarithmic singularity.

Although this procedure is demonstrated here only for S_3 , it can also be successfully applied to any sum or term-by-term integration of a sum which is needed in this problem. One will, however, need the following asymptotic series in closed form:

$$\sum_{n=1}^{\infty} \frac{e^{-nx}}{n} \sin n\lambda = \tan^{-1} \left(\frac{\sin \lambda}{e^x - \cos \lambda} \right), \quad (3.17a)$$

$$\sum_{n=1}^{\infty} e^{-nx} \sin n\lambda = \frac{\sin \lambda}{2(\cosh x - \cos \lambda)}, \quad (3.17b)$$

$$\sum_{n=1}^{\infty} e^{-nx} \cos n\lambda = \frac{\cos \lambda - e^{-x}}{2(\cosh x - \cos \lambda)}, \quad (3.17c)$$

and

$$\sum_{n=1}^{\infty} \frac{e^{-nx}}{n^2} = \frac{\pi^2}{6} + x \ln x - x - \frac{x^2}{4} + \sum_{n=1}^{\infty} \frac{B_{2n} x^{2n+1}}{2n(2n+1)!} \quad (3.17d)$$

where B_i is the i th Bernoulli number as defined by Abramowitz and Stegun (1965, p. 804). In the literature, (3.17a) can be found in Jolley (1961, p. 110-111), (3.17b) and (3.17c) are found in Wheelon (1968, p. 38), and finally, (3.17d) is found in Lewin (1958, p. 246) or Lindelöf (1947, p. 140). In (3.17d), the left side converges well for large x and the right side converges well for small x .

Sample Calculations

Now that the matrix equation has been formulated and methods of computing its elements have been devised, solutions for various cavity and wire configurations can be obtain via numerical solution

on a digital computer. In this section, a few representative solutions are presented.

It should be noted that a similar problem in which the infinite screen is omitted can be solved using a formulation and computer code previously developed (Seidel 1974) to calculate the currents on an array of cylindrical scatters in free space. From these currents, one can easily calculate the electric field in the aperture. Therefore, in addition to solutions of the problem at hand, solutions to the similar problem are presented. These problems are referred to as the flanged and unflanged solutions, respectively, flange meaning the infinite planar screen of the initial problem.

First consider the case of a cavity with a depth (a) of $.6\lambda$ and a width (b) of $.8\lambda$. This cavity has an aperture width of $.6\lambda$ which is centered in the cavity wall ($d = .6\lambda$, $h = .1\lambda$). The cavity is excited by a plane wave with unit magnitude electric field which impinges on the cavity from the negative x direction. Figure 7 shows a plot of aperture field for this cavity for the case of no internal wires. It is seen that the difference between the flanged solution and the unflanged solution is relatively small. Since the interior fields are uniquely determined by the aperture fields, this indicates that the presence of the flanges has little effect upon these interior fields. Note also that the aperture fields go to zero at the edges of the aperture and that they have a maximum magnitude of slightly less than unity. The fields are symmetric about the center of the aperture because of the symmetry of the cavity itself and the symmetry of the incident field.

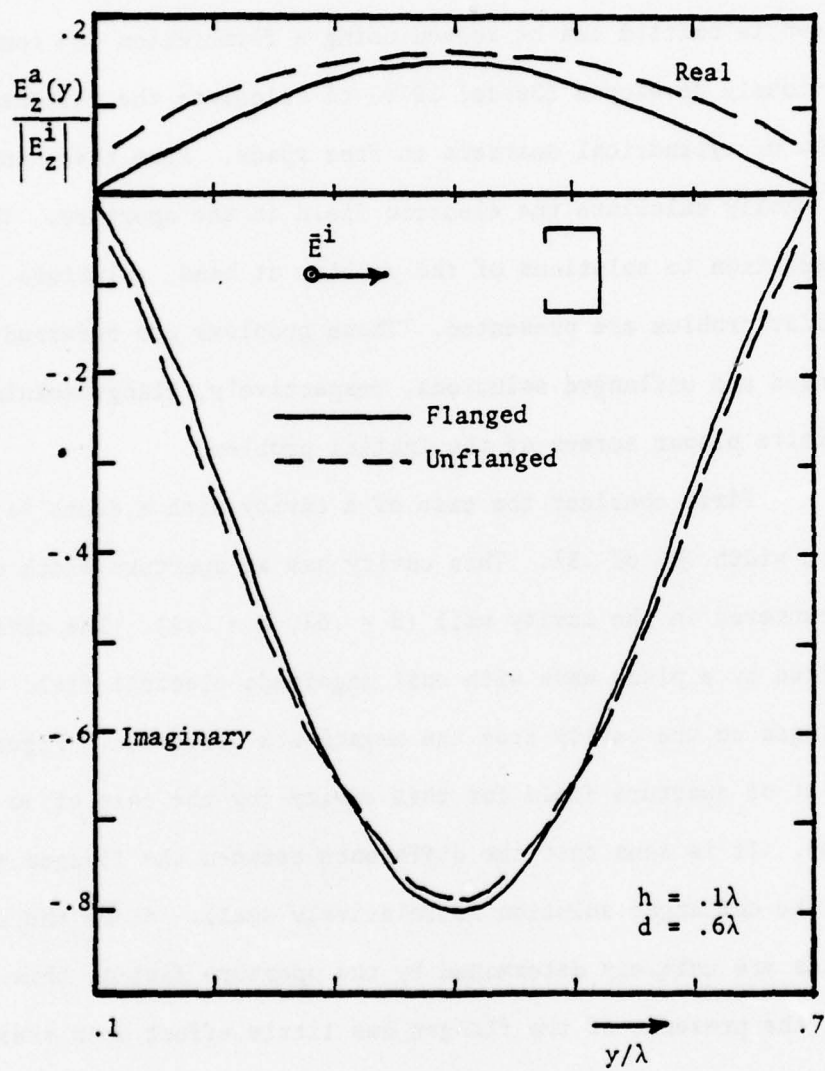


Figure 7. Aperture Field for Cavity with No Interior Wires.

Consider now the same cavity and excitation, but with a wire of radius $.001\lambda$ located at the geometric center of the cavity, $(.3\lambda, .4\lambda)$. Figure 8 shows the aperture field for this case. Again the difference between unflanged and flanged solutions is relatively small. Note that this is also true for the currents excited on the wire, which are $(-1.00 - j 1.48)\text{ma}$ for the unflanged case and $(-.94 - j 1.38)\text{ma}$ for the flanged case. The one significant difference between this solution and that for the case of no wires is that the maximum magnitude of the aperture field is approximately three times larger with the wire than without.

Again consider the same cavity and excitation, but now with two wires of equal radii ($r = .001\lambda$) which are symmetrically located about the center of the cavity at $(.3\lambda, .25\lambda)$ and $(.3\lambda, .55\lambda)$. Figure 9 gives the aperture field for this case. The currents on the two wires are equal due to the symmetry and are $(-.42 - j 1.19)\text{ma}$ and $(-.42 - j 1.25)\text{ma}$ for the unflanged and flanged cases, respectively. The same observations that were made for the case of one wire are also applicable here, except that the peak magnitude of the aperture field is for this case slightly larger.

Finally consider the same cavity and excitation for one centrally located wire ($r = .001$), but with a centered aperture of width $.4\lambda$. The aperture fields for this case are shown in Figure 10. The wire currents are $(.82 - j 1.71)\text{ma}$ and $(.98 - j 1.48)\text{ma}$ for the unflanged and flanged cases respectively. By comparison to Figure 8, it is seen that as a result of shortening the aperture, the magnitudes

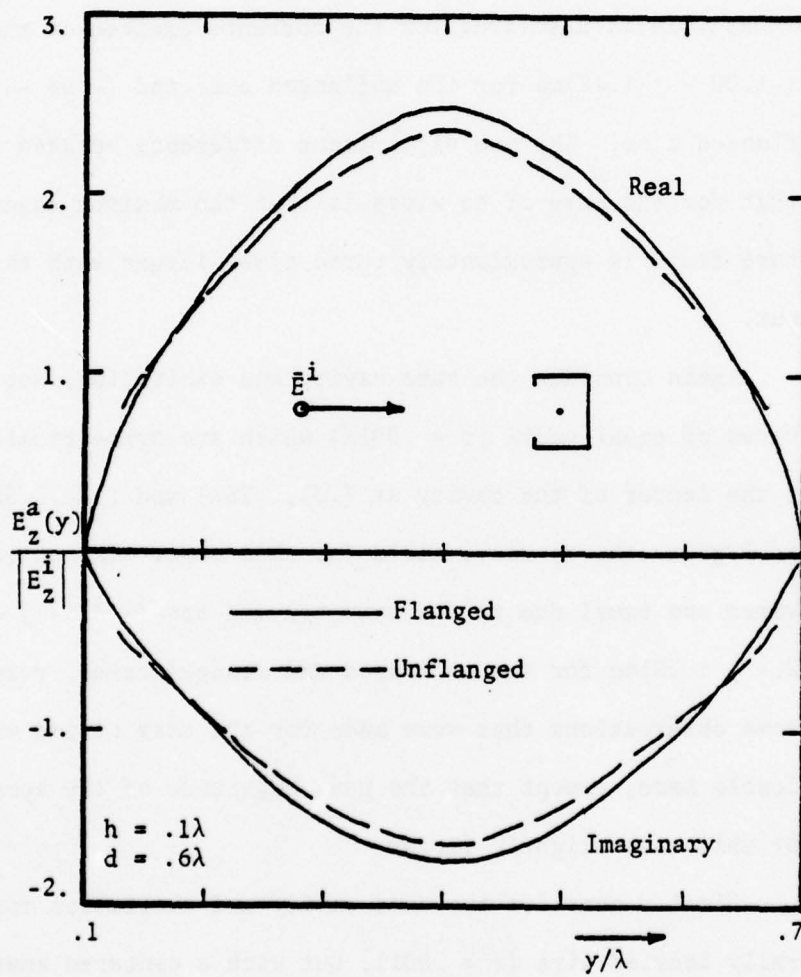


Figure 8. Aperture Field for Cavity with One Interior Wire.

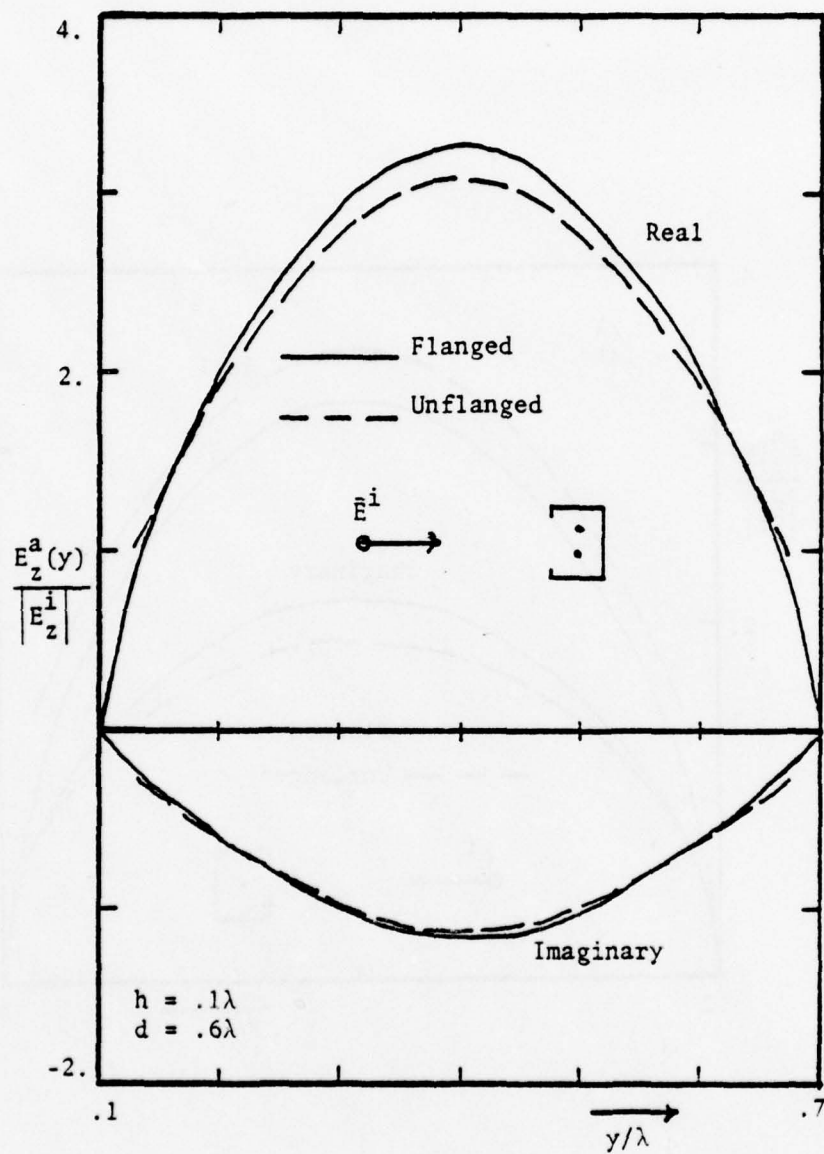


Figure 9. Aperture Field for Cavity with Two Interior Wires.

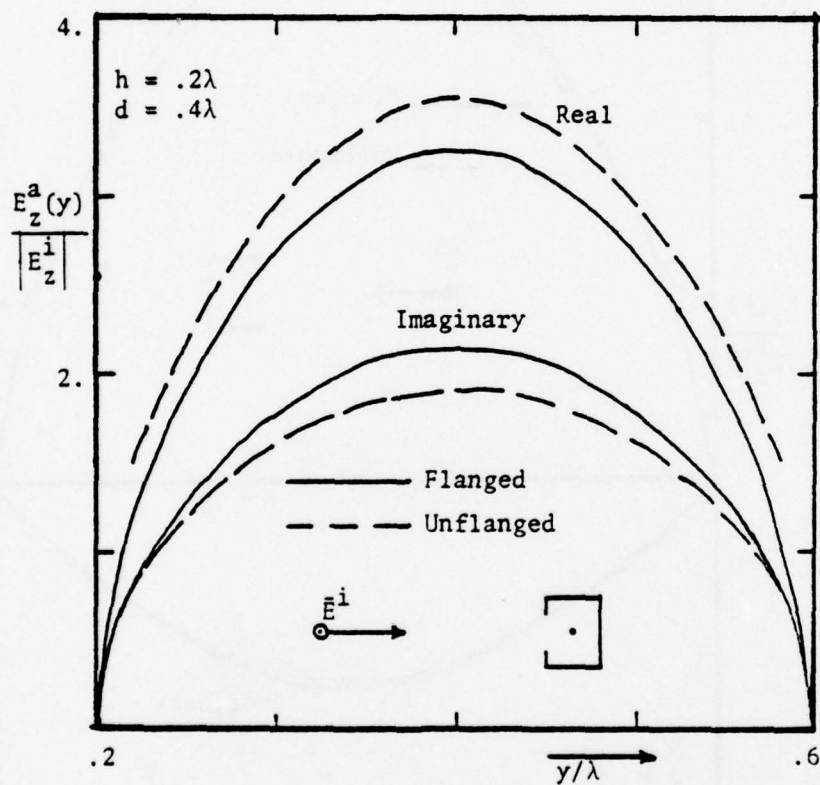


Figure 10. Aperture Field for Cavity with One Interior Wire and $.4\lambda$ Aperture Width.

of the aperture field and current have slightly increased and the phase has changed considerably. Again note that the difference between unflanged and flanged solutions is relatively small.

Final Observations

At this point, a summary of the portions of this two-dimensional problem which will provide insight toward the three-dimensional cavity problem is in order. Such items can be divided into two categories: those which provide insight toward efficient computational methods and those which lead to a better physical understanding of the problem.

First consider those items in the computational category. If the improvement of convergence of the two-dimensional sums is necessary in this problem, then surely it is necessary for the triple sums of the three-dimensional problem. Such techniques as removal of the asymptotic series should be considered, although the amount of work done in the literature on double sums is very small in comparison to that done on single series. Another numerical technique which should be considered is the use of the reduced kernel approximation for the thin wire scatterer. Remember that this approximation removed the necessity of performing an integration of a diverging series.

Secondly, physical insight into the effects of modeling approximations can be gained by noting the one overwhelming result of the data presented. The interior cavity fields and the wire currents are relatively insensitive to the presence of the infinite screen in this two-dimensional analog which is particularly true near resonance

regions. It is quite reasonable to assume that this will also be true for the three-dimensional problem, and thus provides valuable information relating to modeling the three-dimensional cavity problem with or without the infinite screen. This finding is important because it is much easier to consider the problem with an infinite screen than without a screen.

CHAPTER 4

NUMERICAL METHODS FOR CAVITY PROBLEM

Approximation by Matrix Equation

In order to obtain a solution to the integral equation (2.13) for the three-dimensional cavity (with the coupled constraints in (2.21)), it is possible to approximate the integral equation numerically by a matrix equation. This is generally accomplished by the application of the method of moments, which was outlined in Chapter 3.

Consider the integro-differential equation (2.13) for the unknown current $J_z(z)$. It is seen that the differential portion of the operator is the harmonic operator $(\frac{d^2}{dz^2} + k^2)$, which was encountered in (3.1a). Since by thin wire approximations one also knows that the current must vanish at z_u and z_l (the z -coordinates of the wire endpoints, with $z_u > z_l$), the use of piecewise sinusoidal testing functions and pulse expansion functions is indicated (Wilton and Butler 1976), as was the case in the two-dimensional problem. For this problem, these functions are defined by

$$P_q(z) = \begin{cases} 1, & |z - z_q| < \frac{\Delta}{2} \\ 0, & |z - z_q| > \frac{\Delta}{2} \end{cases} \quad (4.1)$$

and

$$\Lambda_p^s(z) = \begin{cases} \text{sinc}(\Delta - |z - z_p|) , & |z - z_p| < \Delta \\ 0 & , \quad |z - z_p| > \Delta \end{cases} \quad (4.2)$$

where $\Delta = (z_u - z_\ell)/(N+1)$ and $z_q = z_\ell + q\Delta$.

Figure 11 illustrates these expansion and test functions. It is important to note that if the wire is attached to the cavity at one or both ends, this choice must be slightly modified because the wire current does not necessarily vanish at the attached end. To rectify this problem, the zero half-pulse at an attached end is replaced by a half-pulse of unknown amplitude. Consequently, a new testing function, which is a half-piecewise sinusoidal function, must be introduced. These are shown in Figure 11 by dashed lines. In the subsequent development of the matrix equation, it is assumed that the wire is unattached. However, the extension to attached wires is straightforward.

Since J_z is assumed to be uniform about the circumference of the wire it is helpful to define the current to be the integral of the current density about circumference of the wire. By this assumption

$$I_z(z) = 2\pi r J_z(z) . \quad (4.3)$$

Now approximate I_z by

$$I_z(z) = \sum_{q=1}^N I_q p_q(z) . \quad (4.4)$$

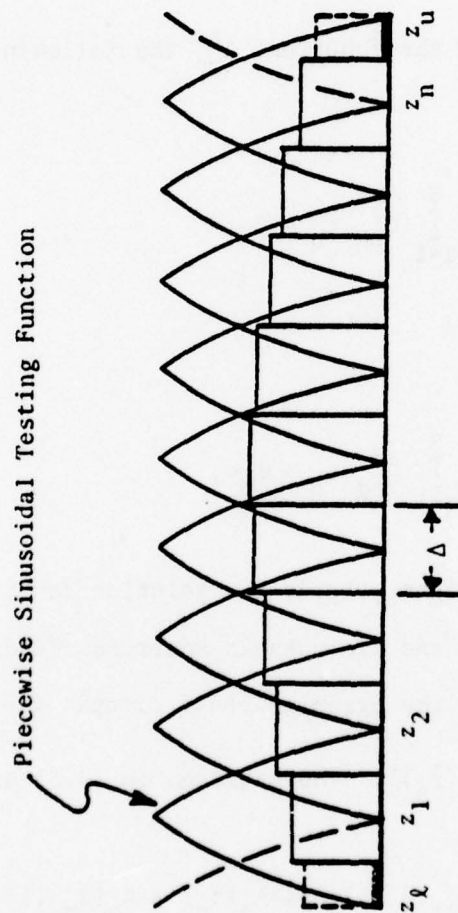


Figure 11. Expansion and Testing Functions for Unknown Wire Currents.

If this is substituted into (2.13) and (2.21) and the inner product defined by

$$\langle u, v \rangle = \int_{z_l}^{z_u} u(z)v(z)dz$$

is taken of (2.13) with the functions Λ_p^s , the following coupled matrix equations are obtained:

$$\sum_{q=1}^N Q_{pq}^a I_q + \sum_{q=1}^3 Q_{pq}^b t_q = 0, \quad (4.5a)$$

$p = 1, 2, \dots, N$, and

$$\sum_{q=1}^N Q_{pq}^c I_q + \sum_{q=1}^3 Q_{pq}^d t_q = E_p, \quad (4.5b)$$

$p = 1, 2, 3$. These functions provide the solution for the unknown current amplitudes $\{I_q\}$ and the unknown aperture fields $(t_1, t_2, t_3) = (E_{T_n}, H_{T_1}, H_{T_2})$ driven by the exterior short circuit fields $(E_1, E_2, E_3) = (E_n^{sc-}(\bar{r}_a), H_1^{sc-}(\bar{r}_a), H_2^{sc-}(\bar{r}_a))$. The matrices in (4.5) are defined by

$$Q_{pq}^a = -j\eta[A_q(z_{p+1}) - 2\cos k\Delta A_q(z_p) + A_q(z_{p-1})], \quad (4.6)$$

$$Q_{p1}^b = C\alpha G_{zn}(\bar{r}_p, \bar{r}_a), \quad (4.7a)$$

$$Q_{p2}^b = -jCk\eta\alpha_{m11} g_{z1}(\bar{r}_p, \bar{r}_a), \quad (4.7b)$$

$$Q_{p3}^b = -jCk\alpha_{m22} g_{e_{z2}}(\bar{r}_p, \bar{r}_a), \quad (4.7c)$$

$$Q_{1q}^c = -\frac{j\eta\Delta}{k} G_{e_{nz}}(\bar{r}_a, \bar{r}_p), \quad (4.8a)$$

$$Q_{2q}^c = \Delta G_{h_{1z}}(\bar{r}_a, \bar{r}_p), \quad (4.8b)$$

$$Q_{3q}^c = \Delta G_{h_{2z}}(\bar{r}_a, \bar{r}_p), \quad (4.8c)$$

and

$$\bar{Q}^d = \begin{bmatrix} 1 + \alpha_e \hat{G}_{enn} & -jk\alpha_{m11} \hat{g}_{en1} & -jk\alpha_{m22} \hat{g}_{en2} \\ \frac{jk}{n} \alpha_e \hat{G}_{h_{1n}} & 1 - \alpha_{m11} \hat{g}_{h_{11}} & -\alpha_{m22} \hat{g}_{h_{12}} \\ \frac{jk}{n} \alpha_e \hat{G}_{h_{2n}} & -\alpha_{m11} \hat{g}_{h_{21}} & 1 - \alpha_{m22} \hat{g}_{h_{22}} \end{bmatrix}. \quad (4.9)$$

where the deleted Green's functions in (4.9) are evaluated at $(\bar{r}, \bar{r}') = (\bar{r}_a, \bar{r}_a)$. Define

$$A_q(z_p) = \int_{\Delta q} K(z_p, z') dz' \quad (4.10)$$

where Δq is the interval $(z_q - \frac{\Delta}{2}, z_q + \frac{\Delta}{2})$ and

$$K(z_p, z') = \frac{1}{2\pi} \int_{-\pi}^{\pi} G_{A_{zz}}(\bar{r}_p, \bar{r}') d\phi', \quad (4.11)$$

where ϕ' is the angular coordinate of a cylindrical coordinate system about the wire axis (Figure 1). Also, $C = 2(1 - \cos k\Delta)$ and \bar{r}_p and \bar{r}' are on the wire surface. Note that to obtain (4.8), the integral over the q th tubular surface segment on the wire has been approximated by the product of the surface area of the segment and the integrand evaluated at a point on the center of the segment.

In order to solve the coupled matrix equations (4.5), one need only obtain a numerical solution to the partitioned matrix equation

$$\begin{pmatrix} \bar{Q}^a & \bar{Q}^b \\ \bar{Q}^c & \bar{Q}^d \end{pmatrix} \begin{pmatrix} \bar{I} \\ \bar{t} \end{pmatrix} = \begin{pmatrix} \bar{0} \\ \bar{E} \end{pmatrix} \quad (4.12)$$

Note that if the effects upon the aperture field of the fields scattered by the wires are ignored, $\bar{Q}^c = \bar{0}$. On the other hand, if the effects of the cavity wall reflections upon the aperture field are ignored $\bar{Q}^d = \bar{I}$, the identity matrix.

However, as in the two-dimensional problem, difficulty arises in attempting to compute the elements of the matrix, each of which contains one of the triply-infinite sums defined in Tables 1 and 2. The computations which exhibit this difficulty can be categorized into three basic types, the first of which is computation of any one of the sums outside the source region. The second category is that of the integral of $G_{A_{zz}}$ over the surface of the wire, for which at one point of the integration $G_{A_{zz}}$ will be divergent. Finally, the deleted Green's functions must be computed at the aperture. The remainder of this chapter attempts to deal with precisely these difficulties.

An Efficient Method of Computing the Sums
Outside the Source Region

As was noted in Chapter 2, each of the Green's functions (Tables 1 and 2) can be reduced from a triple sum to a double sum which is exponentially convergent for $|r-r'| \neq 0$ using (2.8). Indeed, it is easily shown that the asymptotic series associated with any one of these exponentially convergent series is of the form

$$S^{\text{asy}} = \sum_{m,n} f(m,n) \frac{e^{-k_c |z-z'|}}{k_c^\alpha} \quad (4.13)$$

where $k_c^2 = \left(\frac{m\pi}{a}\right)^2 + \left(\frac{n\pi}{b}\right)^2$, $\alpha = 0, 1, 2$ and $f(m,n)$ is a non-exponential function of m and n .

As was found in Chapter 3, it is a good general rule to reduce the triple sum in such a way as to produce the double sum with the most rapid exponential convergence. For example, if

$$\left(\frac{1}{a^2} + \frac{1}{b^2}\right)(z-z')^2$$

is greater than both

$$\left(\frac{1}{b^2} + \frac{1}{c^2}\right)(x-x')^2 \quad \text{and} \quad \left(\frac{1}{a^2} + \frac{1}{c^2}\right)(y-y')^2$$

then the sum over z should be reduced.

Following the lead from the two-dimensional problem in Chapter 3, one would now attempt to find the closed forms of (4.13)

for the various $f(m,n)$ and α . It turns out, however, that the list of double sums for which a closed form is known is painfully short, and does not seem to include (4.13) for any α and $f(m,n)$ of interest in this problem.

Another method which has been suggested is to remove the known singularity from the series by expanding the singularity in the same expansion functions as the series itself. Both Tai and Rozenfeld (1976) and Rahmat-Samii (1975) have removed a delta function singularity from their series for \bar{G}_e in this way. However, this serves little purpose because the known singularity of \bar{G}_e is not the delta function. In fact, as shown by Howard (1974), the singularity of \bar{G}_e is actually the longitudinal portion of $\bar{I}\delta(\bar{r}-\bar{r}')$.

The third alternative, and the one that is used for this work, is to simply sum the double series in an efficient manner. Note that because of the exponential convergence, as one attempts to make this computation nearer and nearer the source, the series will become more and more poorly convergent. Thus one should expect to reach a point such that for $|\bar{r}-\bar{r}'|$ less than some minimum value, numerical computation of the sum in this fashion becomes unfeasible.

However, some things can be done which make this method more efficient. Because of the exponential convergence in the asymptotic series (4.13), one would expect an efficient ordering of terms to be in order of increasing k_c . This takes advantage of the exponential convergence as well as the k_c^α in the denominator. At this point, it is useful to partition the m - n plane with successive curves

(Bromwich, 1926, p.83). If the sum of all terms lying between two successive curves is called s_q , then the double series can be converted into the single series of the form

$$S = \sum_{q=1}^{\infty} s_q .$$

By the proper selection of these curves, the most efficient ordering of terms can be determined.

For this problem such a choice would be that of ellipses with semi-axes in m of $\alpha_q a$ and semi-axes in n of $\alpha_q b$, where α_q is a monotonically increasing sequence of constants. Such a partitioning is shown in Figure 12. Note that for such a choice, each successive partition contains terms for which k_c is larger than in the preceding partition. Also note that since the sum of terms in the q th partition is the q th term of a single infinite series, methods used for determining the convergence of single series can be applied.

To test this method, the sums were numerically computed via digital computer. Figure 13 shows the notation used for the sum. Note that it is assumed without loss of generality that $a \leq b$. Numerically the series was truncated to include only those terms within C_M . The maximum value of m was M . Note that the total number of terms is approximately the area within C_M or $N_T \approx \frac{\pi b}{4a} M^2$. Let $S_p = \sum_{q=1}^p s_q$ and $R_p = \sum_{q=p+1}^{\infty} s_q$. Then R_M is the error resulting from truncation. R_M can be crudely bounded from above with an integral bound. However, for actual computation, convergence was defined to have been

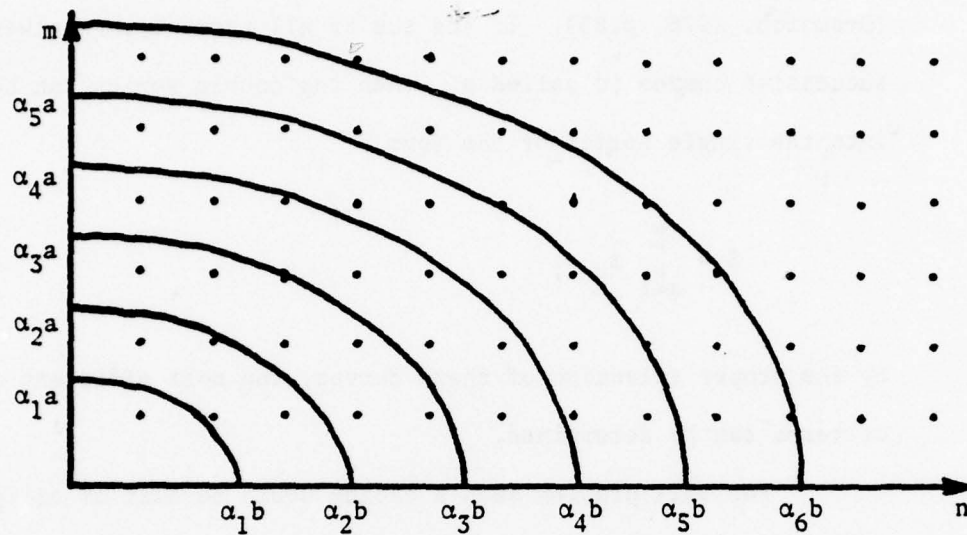


Figure 12. Choice of Contours in m - n Plane for Efficient Summing of Double Series.

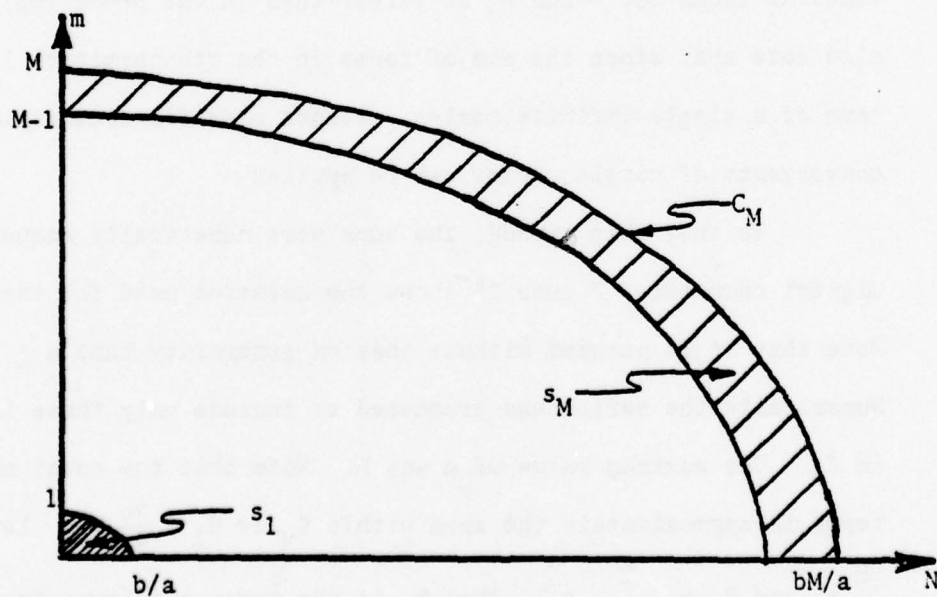


Figure 13. Terms Used in Numerical Computation of Sums.

reached when ratio (s_p/S_p) was less than some small constant C_s for l_s consecutive values of p .

Note that any one of the Green's functions can be reduced to three entirely different double sums. For the purpose of testing, the Green's functions were computed by all three double sums, and then these results were compared. Indeed, the effectiveness of this test is attested to by the several programming errors which it detected. However, once these errors were corrected, extensive testing demonstrated that the three values always agreed to approximately the accuracy specified by the constant C_s . This test also showed that the general rule of reducing the sum so as to give the most rapid exponential convergence did, in fact, produce the particular one of the three possible double sums which required the fewest number of terms.

Finally, extensive testing demonstrated that for cavity sizes in the vicinity of the first resonance, the Green's functions could be easily obtained for values of $|\bar{r}-\bar{r}'|$ greater than $\lambda/20$ (for larger cavities, this minimum distance increases; for smaller cavities, it decreases). Computations at even smaller values of $|\bar{r}-\bar{r}'|$ are not impossible, but rather more and more time consuming.

Numerical Evaluation of the Integral of the Singular Sum

Consider now that evaluation of $A_q(z_p)$, defined by (4.10) and (4.11). As earlier noted, when $p = q$, the integrand $G_{A_{zz}}$ of the integral over the tubular wire surface segment diverges at $\bar{r}_p = \bar{r}'$. Even for $p \neq q$, if p is near q then the integrand will converge poorly. These two difficulties must be overcome.

In order to sidestep the first problem, it would be helpful to apply the reduced kernel approximation (assume all current resides at center of wire). With this approximation, when $p = q$ the integrand would never diverge and, in fact, would be uniformly convergent everywhere on the surface of integration because $|\bar{r} - \bar{r}'| \geq r$. However, one very important consideration is the validity of using the reduced kernel approximation for the kernel (4.11). This kernel is known to include the singularity of the free space kernel plus a remaining smooth homogeneous solution. If $r \ll \lambda$, it is justifiable to assume that the smooth part of K is essentially the same at the center of the wire and at points on the wire surface. Thus one needs a like comparison for the singular portion.

Define K_0 and K_r to be the free space exact and reduced kernels, respectively, given by

$$K_0(\xi) = \frac{1}{2\pi} \int_{-\pi}^{\pi} [\xi^2 + 4r^2 \sin^2 \frac{\phi}{2}]^{-1/2} d\phi \quad (4.14a)$$

and

$$K_r(\xi) = [\xi^2 + r^2]^{-1/2} . \quad (4.14b)$$

Since ultimately integrals of the kernels over ξ are needed, such integrals will be compared. Let

$$\psi_0(z) = \int_0^z K_0(\xi) d\xi = I_0 \quad (4.15a)$$

and

$$\psi_r(z) = \int_0^z K_r(\xi) d\xi = \ln \left[\frac{z}{r} + \left\{ \left(\frac{z}{r} \right)^2 + 1 \right\}^{1/2} \right] \quad (4.15b)$$

where I_0 has been defined by Butler (1975). Figure 14 shows a comparison of these two functions. It is readily apparent that such an approximation is valid for the singular part of the kernel and thus valid for the kernel (4.11).

Using the equation for $G_{A_{zz}}$ from Table 1 (reducing it to a double sum by (2.8b)) and applying the reduced kernel approximation to (4.11), one obtains

$$K(z_p, z') = \frac{4}{ab} \sum_{m,n=1}^{\infty} \frac{\cosh \gamma_c z_c \cosh \gamma_c (c - z_p)}{\gamma_c \sinh \gamma_c c} F(x_c, y_c) \quad (4.16)$$

where $\gamma_c^2 = k_x^2 + k_y^2 - k^2$,

$$F(x_c, y_c) = \text{sink}_{x_c} \text{sink}_{x_p} \text{sink}_{y_c} \text{sink}_{y_p}, \quad (4.17)$$

(x_c, y_c) is the location of the center of the wire and $\bar{r}_p = (x_c + r \cos \phi, y_c + r \sin \phi, z_p)$ is a point on the wire surface. By using a hyperbolic trigonometric identity, one can express (4.16) as the sum of two terms by

$$K(z_p, z') = S(|z_p - z'|) + S(z_p + z') \quad (4.18)$$

where

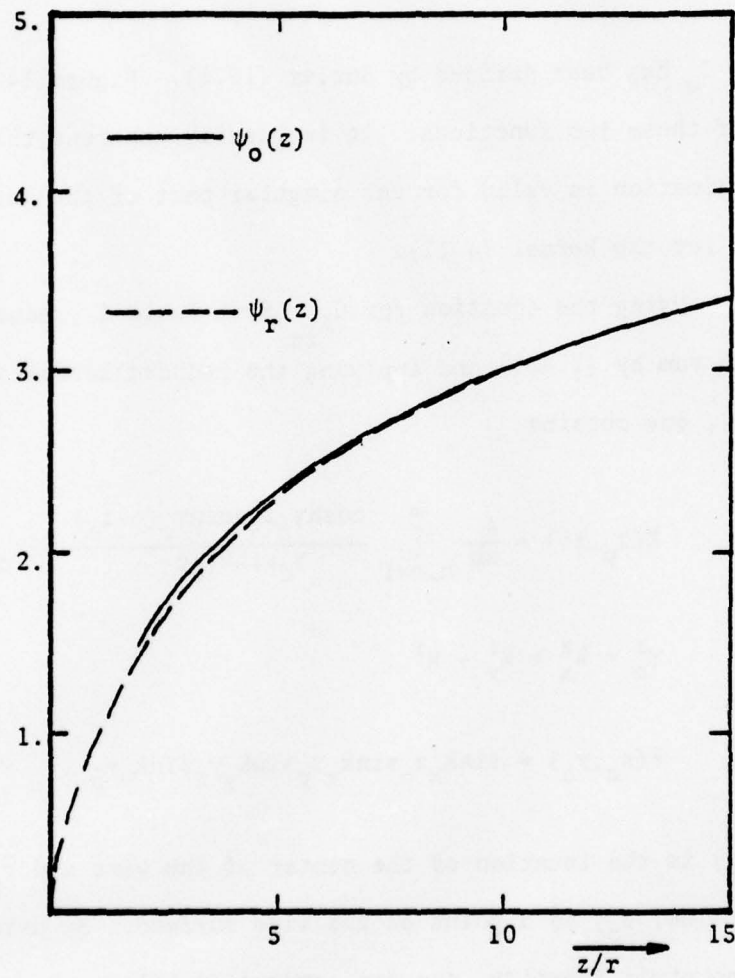


Figure 14. Comparison of the Integrals of the Free Space Exact and Reduced Kernels.

$$S(\beta) = \frac{2}{ab} \sum_{m,n=1}^{\infty} \frac{\cosh \gamma_c (c-\beta)}{\gamma_c \sinh \gamma_c c} F(x_c, y_c) \quad (4.19)$$

To evaluate $A_q(z_p)$ defined by (4.10), one needs to calculate the integral with respect to z' of the kernel (4.18) and thus of (4.19). If this integration is performed on (4.19) term by term, and substituted into (4.18) and (4.10), one finds that

$$A_q(z_p) = Q(|z_p - z_q|) + Q(z_p + z_q) \quad (4.20)$$

where

$$Q(\alpha) = \begin{cases} P(\beta) \Big|_{\beta = \alpha - \frac{\Delta}{2}}^{\alpha + \frac{\Delta}{2}}, & \alpha \geq \frac{\Delta}{2} \\ P(\beta) \Big|_{\beta = 0}^{\frac{\Delta}{2} + \alpha} + P(\beta) \Big|_{\beta = 0}^{\frac{\Delta}{2} - \alpha}, & \alpha \leq \frac{\Delta}{2} \end{cases} \quad (4.21)$$

and where $P(\beta)$ is the indefinite integral of $S(\beta)$ given by

$$P(\beta) = -\frac{2}{ab} \sum_{m,n=1}^{\infty} \frac{\sinh \gamma_c (c-\beta)}{\gamma_c^2 \sinh \gamma_c c} F(x_c, y_c) \quad (4.22)$$

Thus, if $P(\beta)$ can be evaluated for $\beta \geq 0$, then $A_q(z_p)$ can be evaluated on the wire using the reduced kernel.

Consider the case where $\beta = 0$. Note that the hyperbolic sine functions in (4.22) cancel, leaving

$$P(0) = -\frac{2}{ab} \sum_{m,n=1}^{\infty} \frac{\text{sink}_x x_c \text{sink}_x x_p \text{sink}_y y_c \text{sink}_y y_p}{k_x^2 + k_y^2 - k^2} \quad (4.23)$$

It is now recognized that

$$P(0) = -\frac{1}{2} S_3(x_c, x_p, y_c, y_p) \quad (4.24)$$

where S_3 is defined by (3.2c). Thus $P(0)$ can be readily evaluated numerically using (3.16) for $r > 0$. Note that in (4.22), because the hyperbolic sine is an odd function,

$$P(2c - \beta) = -P(\beta) . \quad (4.25)$$

Thus by (4.24) and (4.25) it is also true that

$$P(2c) = \frac{1}{2} S_3(x_c, x_p, y_c, y_p) . \quad (4.26)$$

For $\beta \neq 0$ or $2c$, there appears to be no alternative other than to perform the two-dimensional sum by the methods of the previous section. Note that asymptotically P is of the following form:

$$p^{\text{asy}} \sim \sum_{m,n=1}^{\infty} F \frac{e^{-k_c \beta}}{k_c^2} , \quad 0 < \beta \leq c .$$

Thus for β near zero (or near $2c$, as indicated by (4.25)), poor convergence is expected.

It is known that the reduced kernel (4.16) must contain the singular portion free-space reduced kernel (4.14b) plus a smooth

homogeneous function. By (4.18), $S(\beta)$ must also contain that singularity. If a function $\psi(z)$ is defined similar to (4.15b) by

$$\psi(z) = \int_0^z S(\beta) d\beta = P(z) - P(0) \quad (4.27a)$$

and $\psi_s(z)$ is defined by

$$\psi_s(z) = \psi(z) - \psi_r(z) \quad (4.27b)$$

then ψ_s is the integral of a smooth function and thus itself is smooth.

Since $P(0)$ is readily computed, $\psi(z)$ can be computed numerically for z greater than some minimum value z_0 . Note that the function $\psi_r(z)$ can be calculated by using (4.15b) for any z . Thus $\psi_s(z)$ can be numerically evaluated for $z > z_0$. Note that if ψ_s is smooth and z_0 is sufficiently small, $\psi_s(z)$ can be interpolated for $0 < z < z_0$. Then if $\psi_r(z)$ is added to these interpolated values of $\psi_s(z)$, $\psi(z)$ can be found for $0 < z < z_0$.

To demonstrate the practicality of this technique, consider the curves of Figure 15. They show the functions $\psi(z)$, $\psi_r(z)$ and $\psi_s(z)$ for $0 \leq z \leq .5\lambda$. The cavity dimensions are $a = .7\lambda$, $b = .8\lambda$ and $c = .8\lambda$ with a wire of radius $a = .001\lambda$ located at $x_c = .35\lambda$ and $y_c = .4\lambda$. Note that for $z < .2\lambda$, ψ_s is almost linear and could be interpolated quite accurately. The utility of this method is appreciated if it is noted that for this example the calculation of $P(z)$ took 98 terms at $z = .2\lambda$, 242 terms at $z = .1\lambda$ and 2139 terms at $z = .025\lambda$. In each case, the convergence criteria was $C_s = 10^{-5}$ and $l_s = 3$.

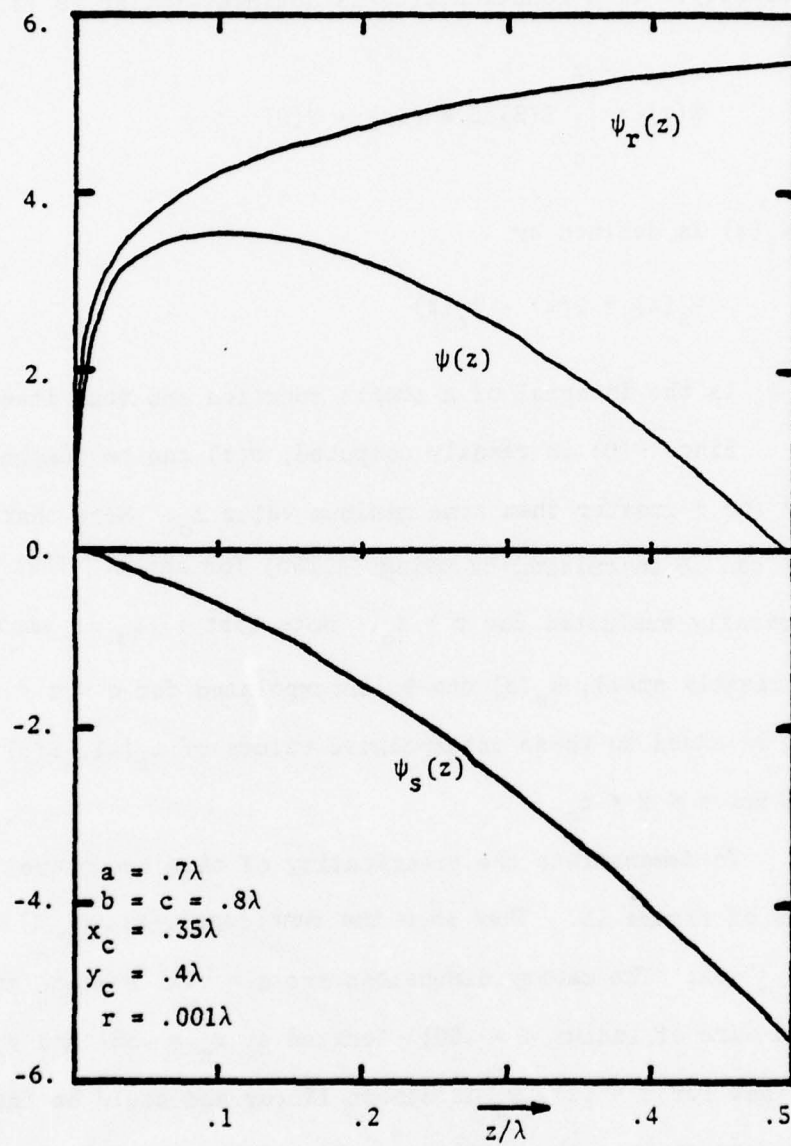


Figure 15. Example Computed Values of $\psi(z)$, $\psi_T(z)$ and $\psi_S(z)$.

Before leaving this section, one important observation should be made. By examination of (4.20), it is seen that $A_q(z_p)$ is a function of two terms, one of which depends only upon $|p-q|$ and the other of which depends only upon $(p+q)$. This means that $A_q(z_p)$ can be calculated for all values of q and p by $3N + 1$ computations rather than $N^2 + 2N$ calculations. Thus for $N \geq 2$, the computing time required can be significantly decreased.

Numerical Evaluation of the Deleted Green's Functions

In the previous sections of this chapter all of the computational difficulties in filling the matrix in (4.12) have been resolved in a workable fashion except for evaluation of the deleted Green's functions in (4.9). These functions, defined by (2.17) and (2.18), must be evaluated at the aperture ($\bar{r}=\bar{r}_a$). Note that although these deleted functions are bounded solutions to the homogeneous wave equation at the point \bar{r}_a , they cannot be calculated directly from (2.17) because both $\bar{G}_A(\bar{r},\bar{r}_a)$ and $\bar{g}_F(\bar{r},\bar{r}_a)$ are divergent at $\bar{r}=\bar{r}_a$.

Ideally, one would like to have expansions for the various free-space dyadic Green's functions so that the singularities could be removed from the cavity dyads term by term, as was discussed earlier in this chapter. The resulting convergent sums would be precisely the deleted Green's functions of (2.17) and (2.18). However, at the present time, practical techniques of employing this method are not available.

In this work, a different approach was taken that relies upon some of the earlier observations of this chapter. Since the deleted Green's functions are homogeneous solutions to the wave equation, it is logical to expect that they could be found by using an interpolation method similar to that employed in the previous section to evaluate $A_q(z_p)$.

Note that such an interpolation scheme would require the evaluation of several different components of the various cavity dyads at points near the source. If it is assumed that the accuracy of the interpolations would improve as the points move nearer the source, increased accuracy would require increased computation time.

Since the double sums in the dyads for the vector potentials converge more rapidly than those for the fields, it is advantageous to compute only the components of \bar{G}_A and \bar{g}_F at several points near the source. Then by (2.17), the associated deleted Green's functions for the vector potentials could be subsequently computed. To find the values of \hat{G}_A and \hat{g}_F in the aperture, an interpolation scheme was employed. To find the values of the other deleted Green's dyads, the differential operators in (2.18) were approximated by finite difference techniques. Note that the points at which the dyads are computed should be chosen carefully so that they provide the proper information for the interpolation and finite difference techniques.

A crucial criterion for the success of this method is the smoothness of the deleted Green's functions. Figure 16 shows plots of $G_{A_{zz}}$ and $\text{Re}(\hat{G}_{A_{zz}})$ as a function of distance from the aperture. Note

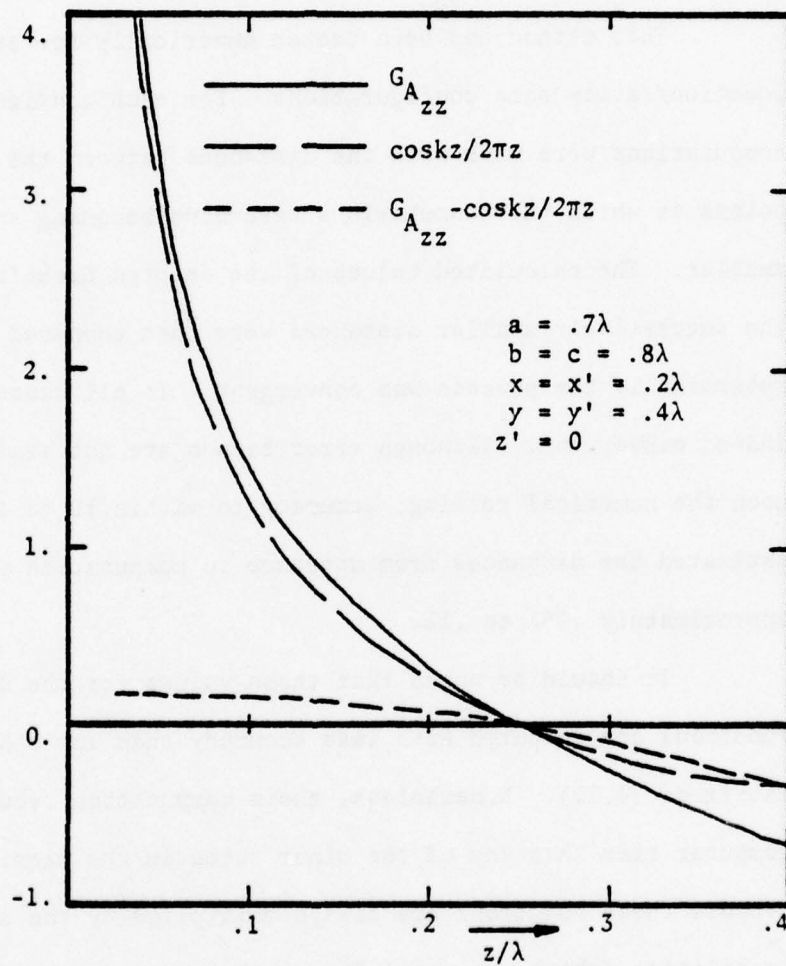


Figure 16. Example Computation for $G_{A_{zz}}$ and the Real Part of $\hat{G}_{A_{zz}}$.

that the deleted function is indeed smooth and could be approximated near the source by interpolation techniques. Figure 17 shows similar plots of $g_{F_{yy}}$ and $\text{Re}(\hat{g}_{F_{yy}})$ and the same observations can be made.

This method has been tested numerically for several aperture location/cavity size configurations. For each configuration, the computations were made with the distances between the aperture and the points at which the computations were made becoming successively smaller. The calculated values of the deleted Green's functions for the successively smaller distances were then compared in order to determine if the process was convergent. In all cases tested, it was indeed convergent. Although error bounds are not available, based upon the numerical testing, accuracy to within 10 to 15 percent is estimated for distances from aperture to computation points being approximately $.05\lambda$ to $.1\lambda$.

It should be noted that these values for the deleted Green's functions are computed with less accuracy than any other terms in the matrix of (4.12). Nonetheless, their computation requires far more computer time than any of the other terms in the matrix. In addition, because these functions are always multiplied by the aperture polarizabilities (which are small for small apertures) in (4.9), they manifest themselves primarily as perturbations and have only a slight effect upon the solution, as will be seen in the following chapter.

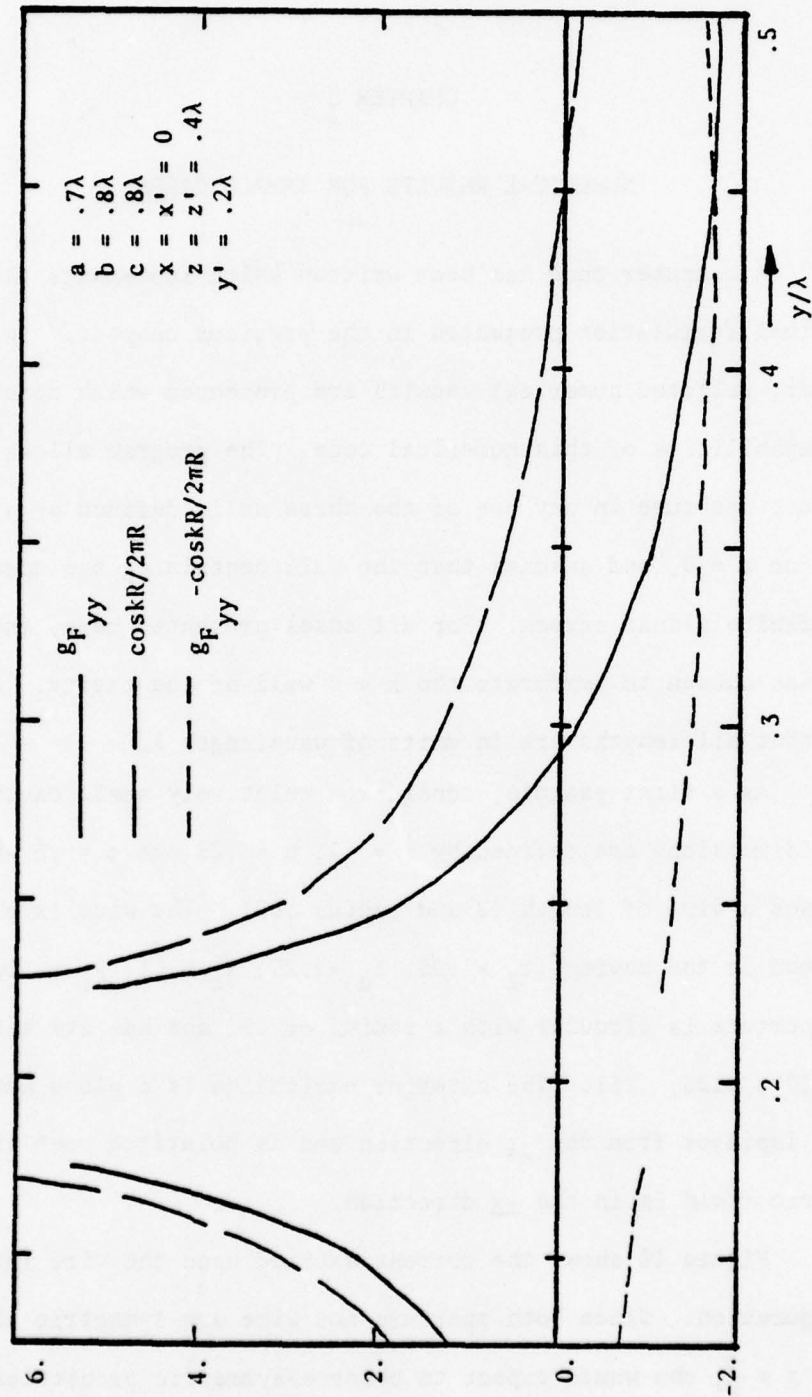


Figure 17. Example Computation of $g_{F_{yy}}$ and the Real Part of $\hat{g}_{F_{yy}}$.

CHAPTER 5

NUMERICAL RESULTS FOR SAMPLE CASES

A computer code has been written which implements the numerical formulation presented in the previous chapter. In this chapter, selected numerical results are presented which demonstrate the capabilities of this numerical code. The program allows for an elliptic aperture in any one of the three walls defined by $x = 0$, $y = 0$ or $z = 0$, and assumes that the wall containing the aperture is an infinite planar screen. For all cases presented here, the aperture was chosen to perforate the $x = 0$ wall of the cavity. Also note that all lengths are in units of wavelength λ .

As a first example, consider a relatively small cavity whose dimensions are defined by $a = .2$, $b = .25$ and $c = .3$ which encloses a wire of length $.2$ and radius $.001$. The wire is exactly centered in the cavity ($z_l = .05$, $z_u = .25$, $x_c = .1$, $y_c = .125$). The aperture is circular with a radius of $.01$ and has its center at $\vec{r}_a = (0., .125, .15)$. The exterior excitation is a plane wave which impinges from the $-z$ direction and is polarized such that the electric field is in the $-x$ direction.

Figure 18 shows the current excited upon the wire for this configuration. Since both aperture and wire are symmetric about the plane $z = \frac{c}{2}$, one would expect to observe symmetric properties in the

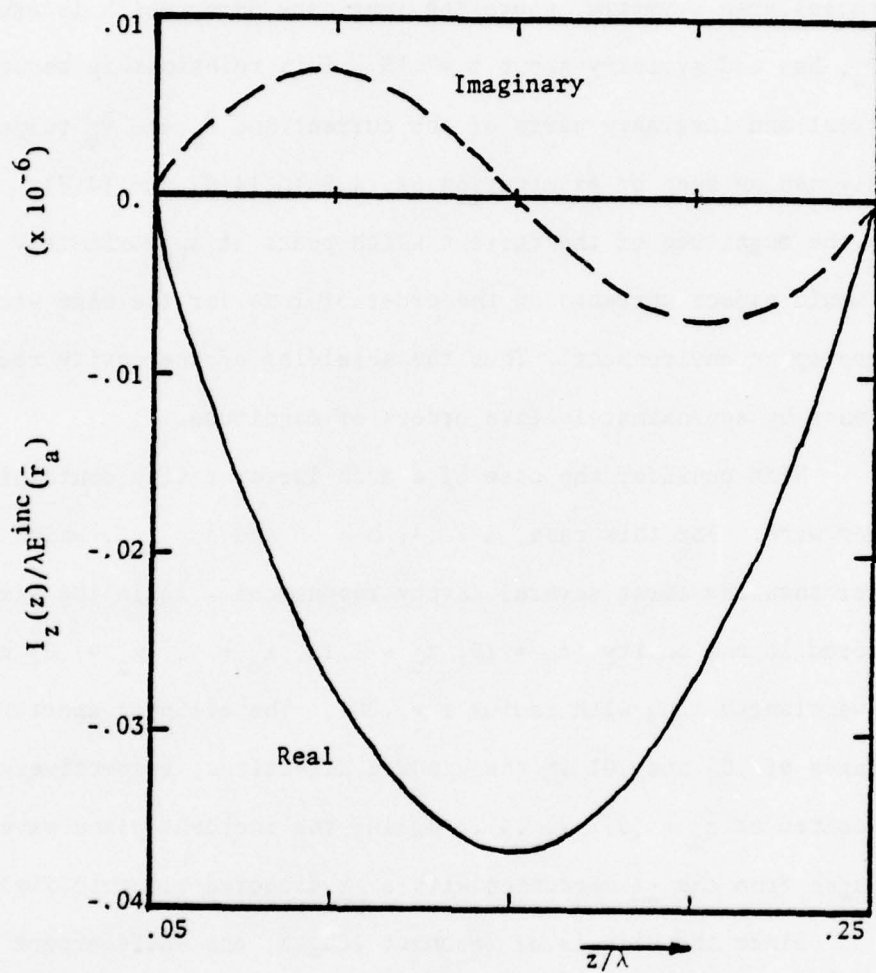


Figure 18. Currents Excited on $.2\lambda$ Wire for a $.2\lambda \times .25\lambda \times .3\lambda$ Cavity.

wire currents. This is indeed the case. The real part of the current, which is excited by the magnetic aperture dipole moment, possesses even symmetry, where the imaginary part, which is excited by \bar{P}_e , has odd symmetry about $z = .15$. This relationship between the real and imaginary parts of the current and \bar{P}_m and \bar{P}_e respectively can be seen by examination of (4.5a), (4.6) and (4.7). Also note the magnitude of the current which peaks at approximately $.04 \mu a$. One would expect currents on the order of 1 ma for the same wire in a free space environment. Thus the shielding of the cavity reduces currents by approximately five orders of magnitude.

Next consider the case of a much larger cavity containing a longer wire. For this case, $a = .4$, $b = .6$ and $c = 1.3$, which is larger than the first several cavity resonances. Again the wire is centered in the cavity ($z_l = .15$, $z_u = 1.15$, $x_c = .2$, $y_c = .3$) and is one wavelength long with radius $r = .001$. The elliptic aperture has semiaxes of $.05$ and $.01$ in the y and z directions, respectively and is located at $\bar{r}_a = (0, .2, .4)$. Again, the incident plane wave impinges from the $-z$ direction with a $-x$ directed electric field.

Since the wire is of resonant length, one would expect to excite resonant currents. Indeed, as shown in Figure 19, this is the case. Also, note that the current magnitude now peaks at approximately $10 \mu a$. This increase over the previous case can be attributed to three causes. First, the aperture is larger and thus more energy is coupled. Second, the wire is of resonant length. Finally,

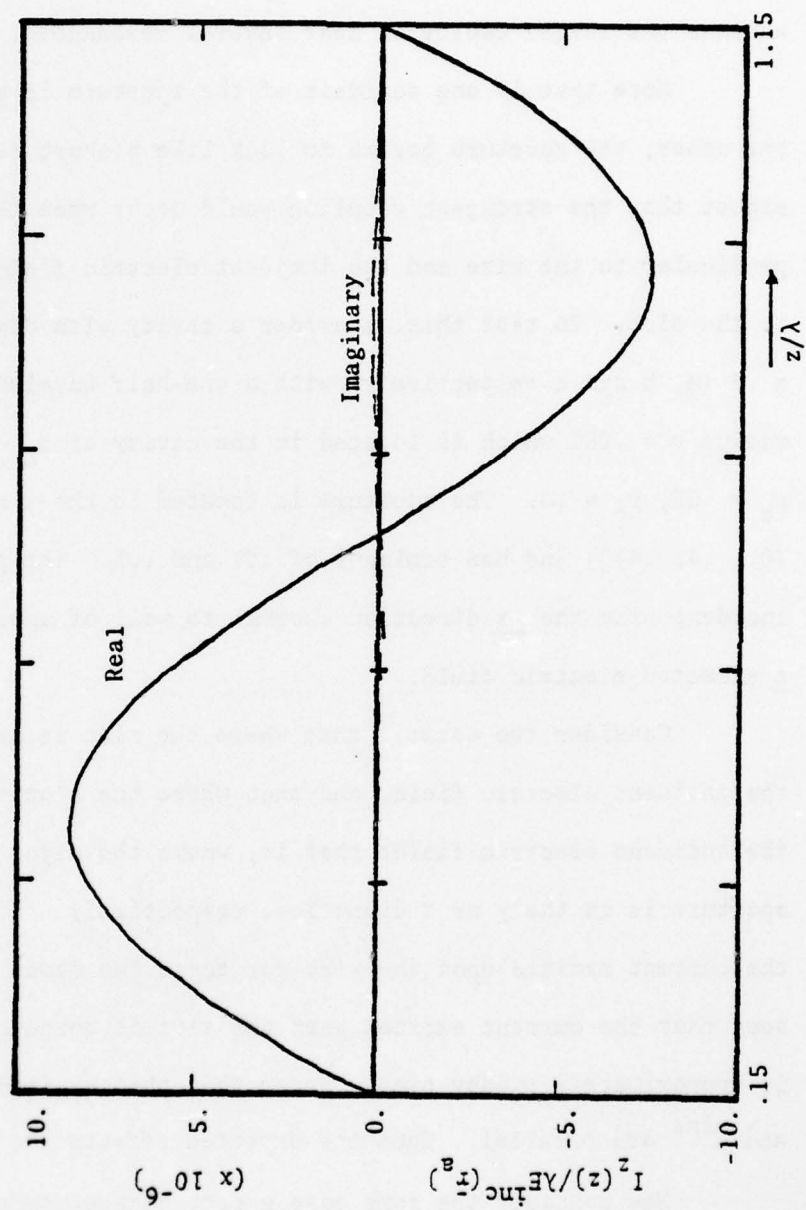


Figure 19. Currents Excited on 1λ Wire in $.4\lambda \times .6\lambda \times 1.3\lambda$ Cavity.

the smaller cavity is considerably below the lowest cavity resonance, whereas the larger cavity is near several resonances.

Note that if one semiaxis of the aperture is much larger than the other, the aperture begins to look like a short slot. One would expect that the strongest coupling would occur when the slot is perpendicular to the wire and the incident electric field is perpendicular to the slot. To test this, consider a cavity with dimensions $.7 \times .7 \times .8$ (a, b and c respectively) with a one-half wavelength wire of radius $r = .001$ which is located in the cavity at $z_l = .15$, $z_u = .65$, $x_c = .35$, $y_c = .4$. The aperture is located in the $x = 0$ wall [$\vec{r}_a = (0., .4, .4)$], and has semiaxes of $.07$ and $.01$. The plane wave is incident from the $-x$ direction (normal to wall of aperture) and has a z directed electric field.

Consider two cases: that where the slot is perpendicular to the incident electric field, and that where the slot is parallel to the incident electric field; that is, where the major semiaxis of the aperture is in the y or z direction, respectively. Figure 20 shows the current excited upon the wire for these two cases. It is readily seen that the current excited when the slot is perpendicular to \vec{E}^{inc} is approximately twenty times larger than that excited when the slot and \vec{E}^{inc} are parallel. Thus the expected effects are observed.

Now consider the same case except change the polarization of the incident plane wave such that the electric field is in the $-y$ direction. Whereas in the previous case the incident electric field was perpendicular to the slot, it is now parallel to the slot, and

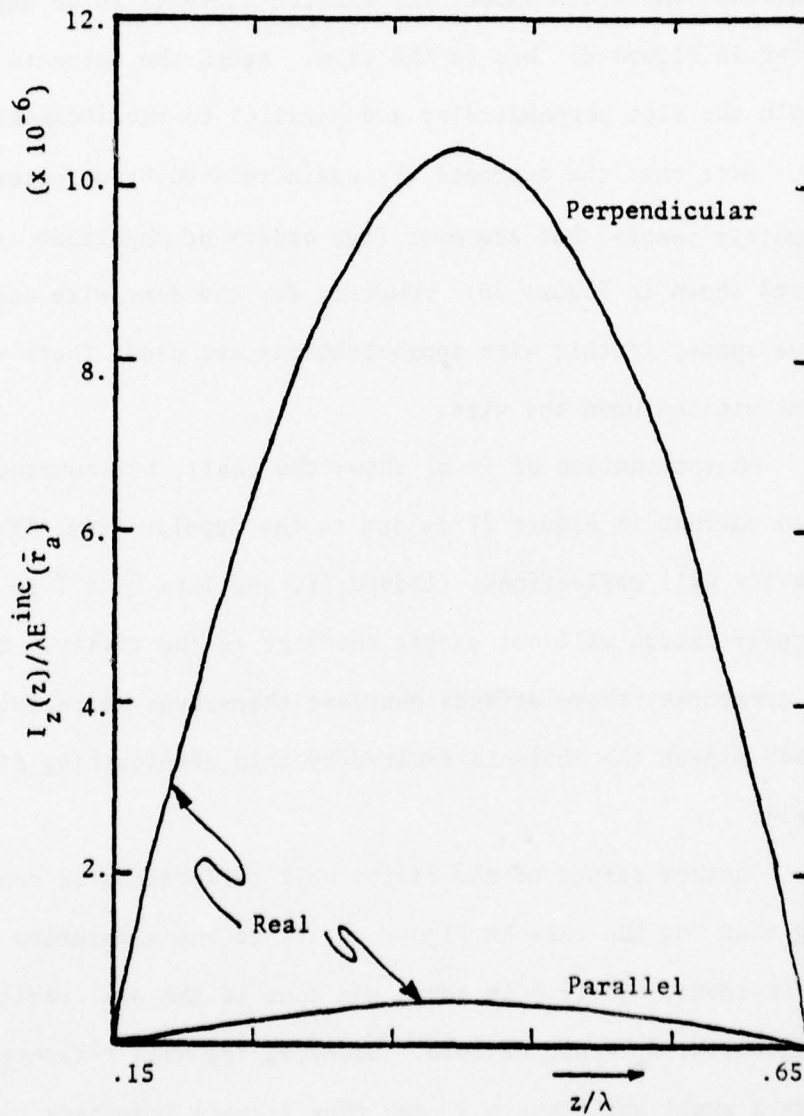


Figure 20. Currents Excited on $.5\lambda$ Wire for Slot Perpendicular and Parallel to \underline{z} Directed Incident Electric Field.

consequently one would expect the excited currents to be much smaller. As shown in Figure 21 this is the case. Again the currents are shown for both the slot perpendicular and parallel to the incident electric field. Note that the currents are again related by a factor of approximately twenty, but are over five orders of magnitude less than the currents shown in Figure 20. However, for the same wire and excitation in free space, if thin wire approximations are used, there will be no current excited upon the wire.

An examination of (4.5) shows the small, but nonetheless nonzero current in Figure 21 is due to the depolarizing effects of the cavity wall reflections. Indeed, if one lets $\bar{Q}^d = \bar{I}$ in (4.5), this polarization will not excite the wire in the cavity. Since for small apertures, these effects manifest themselves as perturbations, one does expect the currents excited by this depolarizing effect to be small.

Another effect of the cavity wall reflections is seen by noting that for the case in Figure 20, since the excitation is normally incident, $E_n^{sc}(\vec{r}_a)$ is zero, and thus if the wall reflections are neglected, \bar{P}_e would be zero. However, the wall reflections produce a small but nonzero \bar{P}_e and thus a small imaginary current. Although not shown in Figures 20 or 21, there was actually an imaginary part of the current, which in all cases was more than two orders of magnitude less than the corresponding real portion.

At this point it is helpful to ascertain the size of this perturbation effect. In order to accomplish this, solutions were

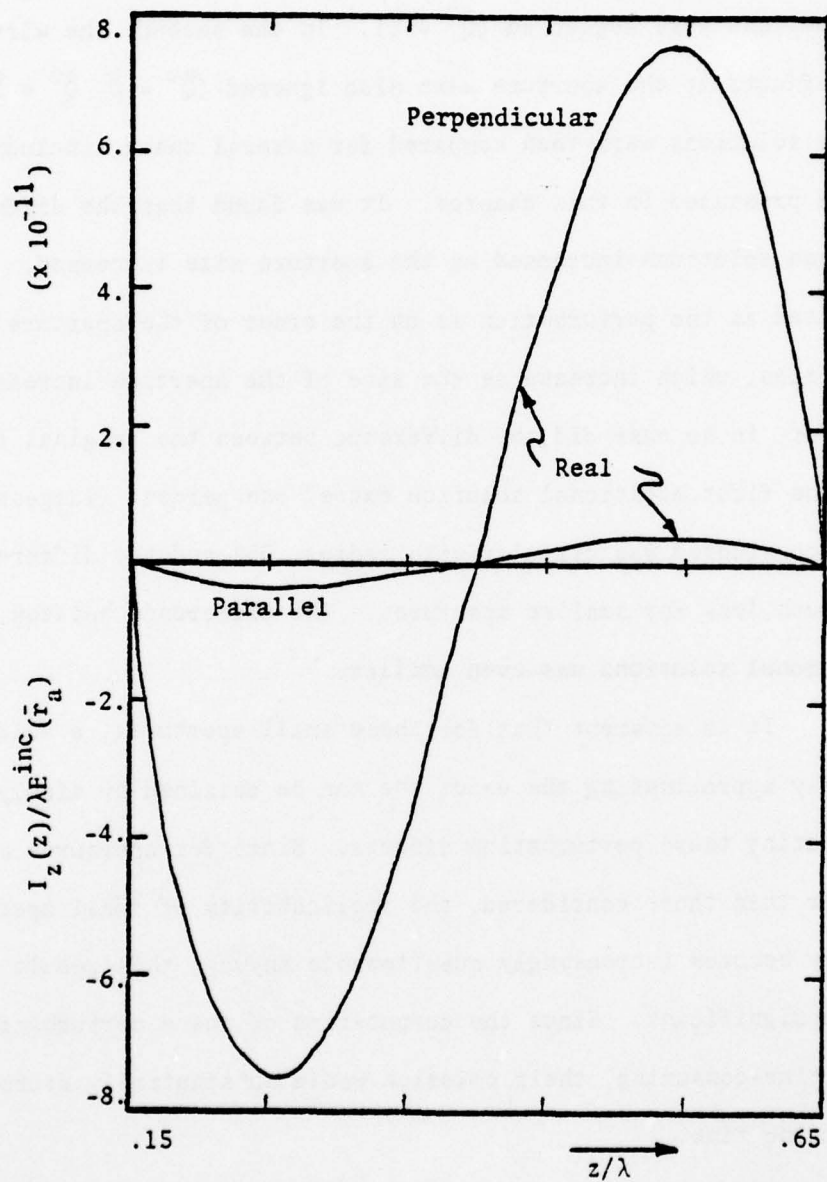


Figure 21. Currents Excited on $.5\lambda$ Wire for Slot Perpendicular and Parallel to $\underline{-y}$ Directed Electric Field.

obtained in two additional manners. In the first, the cavity wall reflections were neglected ($\bar{Q}^d = \bar{I}$). In the second, the wire scattering effects at the aperture were also ignored ($\bar{Q}^c = \bar{O}$, $\bar{Q}^d = \bar{I}$). These solutions were then compared for several cases, including those presented in this chapter. It was found that the difference between solutions increased as the aperture size increased. This is expected as the perturbation is on the order of the aperture polarizabilities, which increase as the size of the aperture increases. However, in no case did the difference between the original solution and the first additional solution exceed one percent (largest aperture considered was circular with radius .05) and the difference was much less for smaller apertures. The difference between the two additional solutions was even smaller.

It is apparent that for these small apertures, a solution closely approximating the exact one can be obtained by simply neglecting these perturbation effects. Since for apertures much larger than those considered, the applicability of small aperture theory becomes increasingly questionable anyway, this result is quite significant. Since the computation of these perturbations are very time-consuming, their omission would substantially decrease computing time.

Finally, consider the case of wires connected to the cavity at one or both ends. Figures 22 and 23 show the wire currents for these two cases respectively. The cavity size is .7 x .8 x .8 and the wire axis is at $(x_c, y_c) = (.15, .5)$ with a wire radius $r = .001$.

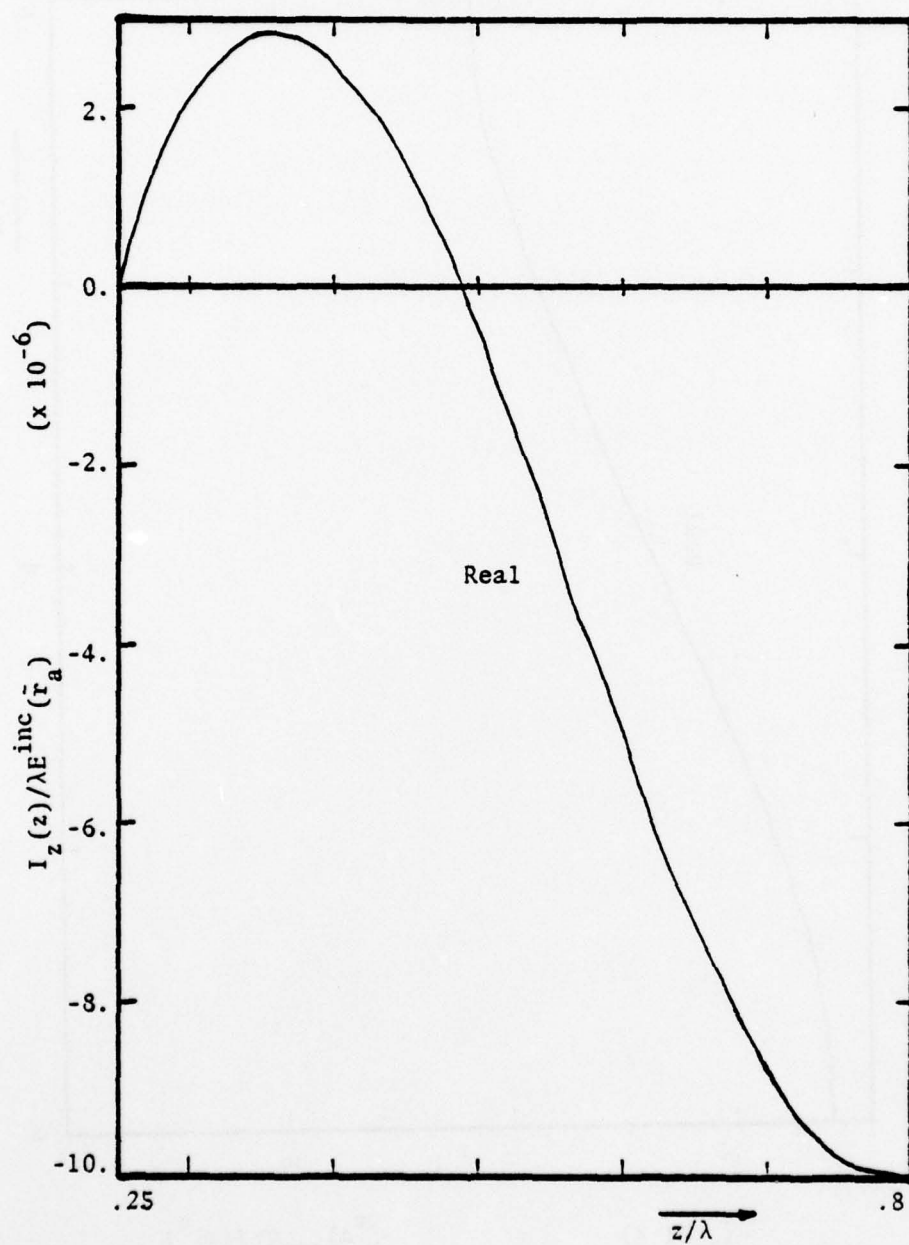


Figure 22. Current Excited on $.55\lambda$ Wire Which Is Attached to Cavity Wall at One End.

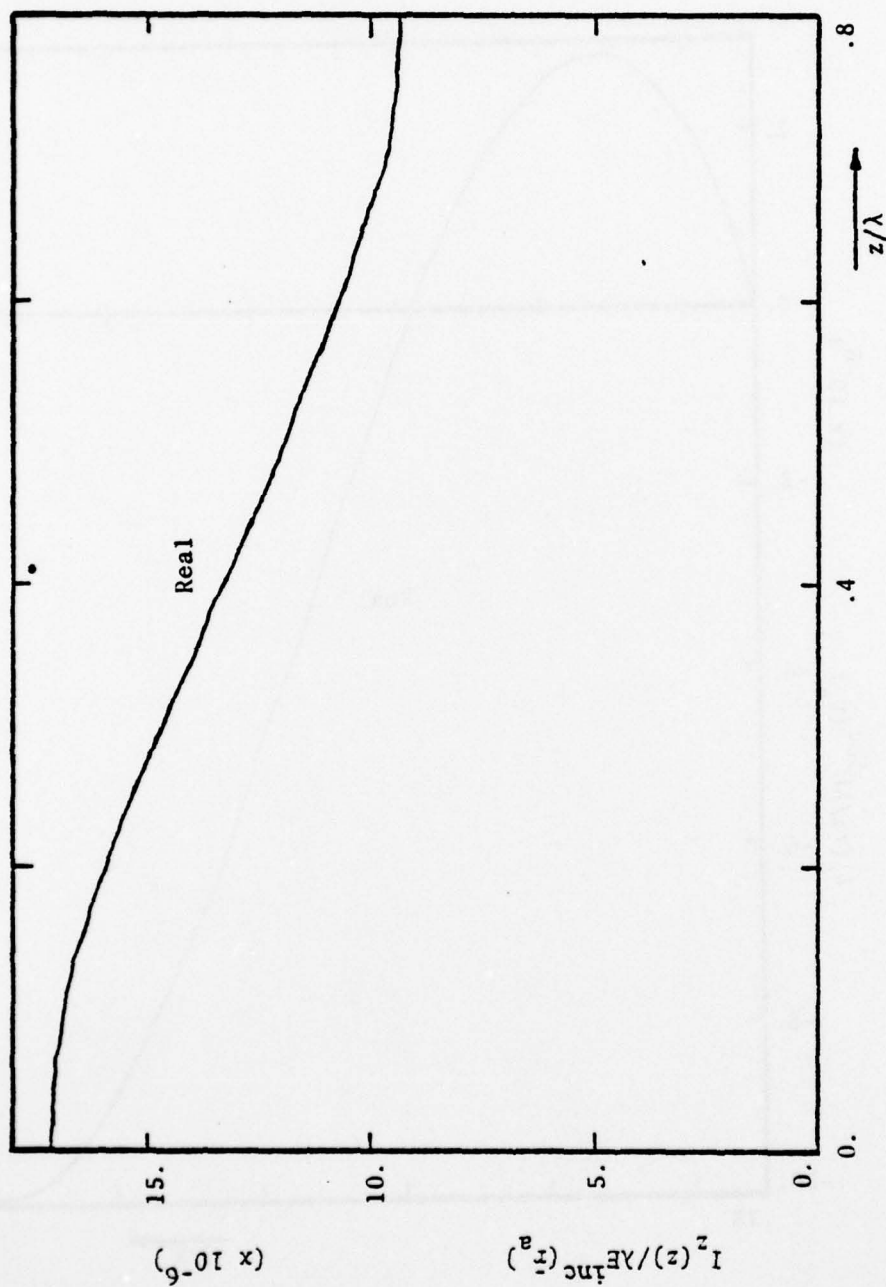


Figure 23. Current Excited on $.8\lambda$ Wire Which Is Attached to Cavity Wall at Both Ends.

The aperture is located at $\vec{r}_a = (0., .3, .6)$ and its semiaxes in the y and z directions are .07 and .01 respectively. The plane wave is normally incident upon the aperture from the -x direction and the electric field is z directed.

In Figure 22 the wire is connected at $z = .8$ and as expected, the axial (z) derivative of the current goes to zero at the wall. Also, as expected, the current at the free end of the wire vanishes. Similarly in Figure 23, where the wire is connected at both ends of the cavity, the axial derivative of the current vanishes at both $z = 0$ and $z = .8$. In both cases, the current magnitudes are on the order of 10 μ a. For a similar cavity and excitation, but having a free wire (Figure 20, perpendicular slot) the current magnitude is also of this order.

Thus it has been shown that physically reasonable numerical solutions can be obtained for a variety of cavity/aperture/wire configurations. It should be noted however that important comparisons between theory and experiment must await the publishing of experimental results applicable to this problem. Such comparisons would demonstrate the applicability of the modeling and the accuracy of the solution.

CHAPTER 6

CONCLUSION

In this paper, the task was undertaken to formulate and numerically solve the problem of an aperture excited wire scatterer in a rectangular cavity. The formulation in Chapter 2, although tedious, was relatively straightforward. It was found that the major difficulties of the problem lay in the numerical evaluation of the infinite double sum Green's functions for the cavity interior.

By considering the preliminary two-dimensional problem in Chapter 3, valuable insight was obtained toward resolving the numerical difficulties of the three-dimensional problem. It is important to realize that the two-dimensional problem is also a significant problem in and of itself. Two-dimensional problems in many cases provide adequate models for more complex three-dimensional structures. In addition, solutions to this problem have the advantage of being applicable to large apertures whereas the major solution herein is restricted to small apertures only.

The real significance of this work is contained in Chapter 4. Here it was demonstrated that the dyadic Green's functions for the cavity problem can be calculated (although in some cases, only with considerable effort). This finding is particularly essential in or near the source region. This is because the treatment of the singular

kernel of an integral equation in the source region is crucial to its numerical solution. Thus the ability to numerically solve the integral equation for a scatterer in a cavity is demonstrated, and indeed, numerical results can be provided as found in Chapter 5.

Suggested Extensions of this Work

Perhaps more important than what this work has accomplished is rather what extensions and applications can be found for it. In general, the most immediate extensions of this work would be to eliminate some of the restrictions caused by the initial assumptions of the problem. The relevance of an extension can thus be measured by asking how restrictive is the assumption which the extension eliminates.

A very important extension would be to allow a large aperture in the cavity wall. It should be noted that in order to do this an aperture field integral equation must be formulated and solved simultaneously with the integral equation for the wire (2.13). In general, the aperture fields must be divided into a two-dimensional array of surface patches, requiring large amounts of computer storage and time. However if the aperture is small in one dimension (a slot), it need only be divided into a one-dimensional array of surface patches.

A second extension of the present work would be to account for more complex scattering geometries. This might include uniformly or lumped loaded wires, more than one wire, or wires which are not parallel to one of the coordinate axes. The first two of these suggestions would be relatively straightforward (but only if each wire remains

parallel to one of the coordinate axes) and would primarily require extensive logic for their numerical implementation.

It should be noted, however, that the consideration of a wire which is not parallel to one of the coordinate axes would require considerable effort. First of all, integral equation (2.12) would have to be used, and thus all none components of the dyads would be needed. In addition, the benefits of piecewise-sinusoidal testing (namely, the removal of the differential operator) are no longer applicable. Probably the most important problem this extension would cause, is that the methods outlined in Chapter 4 for evaluating the integral of the kernel could no longer be applied. Careful examination reveals that this technique is crucially dependent upon the fact that the wire is z-directed.

Finally, consider the application of this work to the case of transient excitation such as an EMP and characterize the response of the aperture and its coupling to the wire within the cavity, based on the obvious application of the singularity expansion method (Baum 1971), which allows one to express the total response in terms of few parameters via, the natural frequencies, natural modes and coupling coefficients. Or one can follow the direct procedure to obtain the time dependent solution by inverse Fourier transformation. Note that this would involve the use of the time-harmonic solution at many angular frequencies ω over the spectrum of the excitation. It should be noted that for many

transient excitations (including EMP) the low frequency portion of the spectrum is dominant. Thus for such excitations, a quasi-static solution for the problem is needed for small ω in order to perform the inverse Fourier transform numerically.

LIST OF REFERENCES

- Abramowitz, M. and I. Stegun. Handbook of Mathematical Functions, New York: Dover, 1965.
- Baum, C. E. "On the Singularity Expansion Method for the Solution of Electromagnetic Interaction Problem," AFWL Interaction Note #88, Dec 76.
- Bethe, A. A. "Theory of Diffraction by Small Holes," Phys. Revs., Vol. 66, pp. 163-182, Oct. 1944.
- Bouwkamp, C. J. "Diffraction Theory," Repts. Prog. in Phys., Vol 17, pp. 35-100, 1954.
- Bromwich, T. J. I'A. An Introduction to the Theory of Infinite Series, 2nd Ed., London: MacMillan, 1926.
- Butler, C. M. "Evaluation of Potential Integral at Singularity of Exact Kernel in Thin-Wire Calculations," IEEE Trans. on Ant. and Prop., Vol. AP-23, pp. 293-295, March 1975.
- Butler, C. M. and K. R. Umashankar. "Electromagnetic Excitation of a Wire Through an Aperture-Perforated, Conducting Screen," IEEE Trans. Ant. Prop., Vol. AP-24, pp. 456-462, July 1976.
- Butler, C. M. and D. R. Wilton. "Analysis of Various Numerical Techniques Applied to Thin-Wire Scatterers," IEEE Trans. on Ant. and Prop., Vol. AP-23, pp. 534-540, July 1975.
- Cheng, D. K. and C. A. Chen. "On Transient Electromagnetic Excitation of a Rectangular Cavity Through an Aperture," Air Force Weapons Laboratory, Rept. AFWL-TR-75-91, June 1976.
- Cohn, S. B. "Determination of Aperture Parameters by Electrolytic-Tank Measurements," Proc. IRE, Vol. 39, pp. 1416-1421, Nov. 1951.
- Cohn, S. B. "The Electric Polarizability of Apertures of Arbitrary Shape," Proc. IRE, Vol. 40, pp. 1069-1071, Sept. 1952.
- Collin, R. E. Field Theory of Guided Waves, New York: McGraw-Hill, 1960.
- Collin, R. E. "On the Incompleteness of E and H Modes in Wave Guides," Can. J. Phys., Vol. 51, pp. 1135-1140, June 1973.
- DeMeulenaere, F. and J. Van Bladel. "Polarizability of Some Small Apertures," IEEE Trans. Ant. Prop., Vol. AP-25, pp. 198-205, March 1977.

AD-A059 812

ARIZONA UNIV TUCSON

F/G 20/14

EXCITATION OF A WIRE IN A RECTANGULAR CAVITY. VOLUME I. THEORY.(U)

MAY 78 D B SEIDEL

AFOSR-76-3009

UNCLASSIFIED

AFWL-TR-77-221-VOL-1

NL

2 OF 2
AD
A059812



END
DATE
FILMED
12-78

DDC

- Teichmann, T. "Completeness Relations for Loss-Free Microwave Junctions," J. Appl. Phys., Vol. 23, pp. 701-710, July 1952.
- Teichmann, T. and E. P. Wigner. "Electromagnetic Field Expansions in Loss-Free Cavities Excited Through Holes," J. Appl. Phys., Vol. 24, pp. 262-267, March 1953.
- Titchmarsh, E. C. The Theory of Functions, 2nd Ed., London: Oxford University Press, 1939.
- Tsai, L. L., D. G. Dudley and D. R. Wilton. "Electromagnetic Scattering by a Three-Dimensional Conducting Rectangular Box," J. Appl. Phys., Vol. 45, Oct. 1974.
- Weyl, H. "Über Die Randwertaufgabe der Strahlungstheorie und Asymptotische Spektralgesetze," J. F. Reine Ange. Math., Vol. 143, pp. 177-202, 1913.
- Weyl, H. "Das Asymptotische Verteilungsgesetz der Eigenschwingen Eines Beliebigen Gestalteten Elastischen Körpers," Rend. d. Circ. Math. Palermo, Vol. 39, pp. 1-49, 1915.
- Wheelon, Albert D. Tables of Summable Series and Integrals Involving Bessel Functions, San Francisco: Holden-Day, 1968.
- Wilton, D. R. and C. M. Butler. "Efficient Numerical Techniques for Solving Pocklington's Equation and Their Relationships to Other Methods," IEEE Trans. Ant. and Prop., Vol. AP-24, pp. 83-86, January 1976.

- Hansen, W. W. "A New Type of Expansion in Radiation Problems," Phys. Rev., Vol. 47, pp. 139-143, 1935.
- Harrington, R. F. Time-Harmonic Electromagnetic Fields, New York: McGraw-Hill, 1961.
- Harrington, R. F. Field Computation by Moment Methods, New York: MacMillan, 1968.
- Howard, A. Q., Jr. "On the Longitudinal Component of the Green's Function Dyadic," Proc. IEEE (Lett.), Vol. 62, pp. 1704-1705, Dec. 1974.
- Jolley, L. B. W. Summation of Series, 2nd Ed., New York: Dover, 1961.
- Kurokawa, K. "The Expansion of Electromagnetic Fields in Cavities," IRE Trans. MTT, Vol. MTT-6, pp. 178-187, April 1958.
- Lewin, L. Dilogarithms and Associated Functions, London: MacDonald, 1958.
- Lewin, L. Theory of Waveguides, New York: Halsted Press, 1975.
- Lindelof, Ernst. Le Calcul des Residus et ses Applications a la Theorie des Fonctions, New York: Chelsea, 1947.
- Morse, P. M. and H. Feshbach. Methods of Theoretical Physics, Part II, New York: McGraw-Hill, 1953.
- Rahmat-Samii, Y. "On the Question of Computation of the Dyadic Green's Function at the Source Region in Waveguides and Cavities," IEEE Trans. on MTT, Vol MTT-23, pp. 762-765, Sept. 1975.
- Seidel, D. B. "A New Method for the Detection and Correction of Errors Due to Interior Resonance for the Problem of Scattering from Cylinders of Arbitrary Cross-Section," Master's thesis, Department of Electrical Engineering, University of Arizona, Tucson, Arizona, Dec. 1974.
- Seidel, D. B. and C. M. Butler. "Determination of Current on a Wire which Passes Through a Hole in a Planar Screen," URSI Annual Meeting, Amherst, Massachusetts, Oct. 1976.
- Tai, C. T. "On the Eigenfunction Expansion of Dyadic Green's Functions," Proc. IEEE (Lett.), Vol. 61, pp. 480-481, April 1973.
- Tai, C. T. and P. Rozenfeld. "Different Representations of Dyadic Green's Functions for a Rectangular Cavity," IEEE Trans. on MTT, Vol. MTT-24, pp. 597-601, Sept. 1976.